REPORT NO. 91

EXPERIMENTS ON TURBULENT BOUNDARY LAYERS ALONG A CIRCULAR CYLINDER WITH AND WITHOUT SEPARATION

HANS FERNHOLZ
PAUL GIBSON

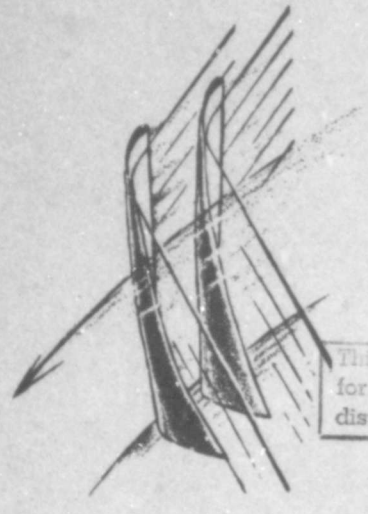

Research was carried out under the Bureau of Ships General Hydromechanics Research Program, S-R009 01 01, Administered by the David Taylor Model Basin

Contract Nonr 1841(91)

AUGUST 1967

GAS TURBINE LABORATORY
MASSACHUSETTS INSTITUTE OF TECHNOLOGY
CAMBRIDGE, MASSACHUSETTS 02139

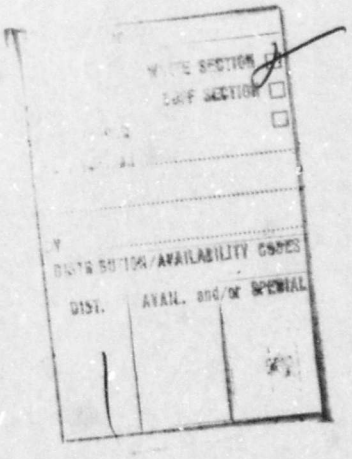

EXPERIMENTS ON TURBULENT BOUNDARY LAYERS ALONG A CIRCULAR CYLINDER WITH AND WITHOUT SEPARATION

by

Hans Fernholz

Paul Gibson

Research carried out under Bureau of Ships
General Hydromechanics Research Program, S-R009 01 01,
administered by the David Taylor Model Basin

Contract Nonr 1841(91)

REPORT NO. 91

Gas Turbine Laboratory

Massachusetts Institute of Technology

July 1967

SUMMARY

Experiments were conducted in a turbulent boundary-layer near separation along a circular cylinder with the flow in the axial direction. The pressure gradient along the axis of the cylinder could be varied such that it was possible to maintain three boundary-layer configurations close to separation or with regions of reversed flow:

1. A turbulent boundary-layer with skin friction zero.

2. A turbulent boundary layer with a separated region and reattachment further downstream with skin friction zero.

3. A turbulent boundary layer with a region of small but constant skin friction and normal separation.

Pressure and skin friction along the cylinder wall, as well as mean velocity profiles in the boundary-layer, were measured.

ACKNOWLEDGEMENTS

This work was done during the academic year 1966/67 at the Gas Turbine Laboratory using the existing experimental apparatus designed by P. Goldberg and H. L. Moses.

We are deeply grateful to Professor E. S. Taylor, the director of the Laboratory, for his hospitality and for many stimulating discussions of the experiments. The pleasant atmosphere and working conditions of the Gas Turbine Laboratory were greatly enjoyed. Professor D. G. Wilson's help was appreciated for editing the manuscript. We finally wish to thank Miss Lotte Wiedmann for assisting with the typing.

The stay of the first author in Cambridge was made possible under the exchange scheme between the Technische Universitaet Berlin and the Massachusetts Institute of Technology.

The numerical calculations were done with the assistance of the M.I.T. Computation Center.

TABLE OF CONTENTS

LIST OF FIGURES

NOMENCLATURE

A	Constant in the "law of the wall"
B	Constant in the "law of the wall"
C_f	Wall friction coefficient $2\tau_w/\rho u_\delta^2$
d	Diameter of Preston tube
H_{12}	Shape factor δ_1/δ_2
H_{32}	Shape factor δ_3/δ_2
R	Radius
Re_x	Reynolds number based upon x
Re_{δ_2}	Reynolds number based upon momentum thickness $\rho\, u_\delta\, \delta_2/\mu_w$
u	Component of mean velocity parallel to the wall
u_δ	Free stream velocity
$(u_\delta)_o$	Free stream velocity at the first pressure tap
u_τ	Skin friction velocity $(\tau_w/\rho)^{1/2}$
u'	Component of turbulent velocity fluctuation in x-direction
v'	Component of turbulent velocity fluctuation in y-direction
x	Coordinate parallel to the wall
y	Coordinate perpendicular to the wall
z	Coordinate along circumference
δ	Boundary layer thickness
δ_1	Displacement thickness } see Chapter 2.3
δ_2	Momentum thickness } see Chapter 2.3
δ_3	Energy thickness } see Chapter 2.3
Δp	Pressure drop
μ	Dynamic viscosity
ν	Kinematic viscosity
ρ	Density
$\rho\overline{u'v'}$	Reynolds shear stress
τ_w	Wall shear stress

1. INTRODUCTION

During the last eight years a number of experiments on turbulent boundary layers with pressure gradient have been published, most of them dealing with extreme flow conditions. The flow configurations investigated were equilibrium boundary layers (Bradshaw and Ferris[1], Bradshaw[2], Herring and Norbury[3]), boundary layers with strong adverse pressure gradients, and boundary layers with zero skin friction. The pressure gradients set up showed two main features. A monotonic pressure rise led to separation of the boundary layer some distance downstream (Schubauer and Spangenberg[4], Moses[5], and Perry[6]). If the adverse pressure rise was reversed just before the flow reached separation, the separated state could be avoided (Moses[7], Goldberg[8]).

The third species of boundary-layer flow was illustrated by two experiments (Stratford[9], Spangenberg, Rowland, Mease[10]). There the pressure distribution was adjusted in such a way that the turbulent boundary layer remained on the point of separation for some distance without separating. In both cases the skin friction was assumed to be close to zero which was concluded from the behavior of wool tufts along the wall. Despite this rather critical condition of the boundary-layer it could thus be proved that such a boundary-layer flow is stable and can be maintained over longer distances ($x_{sep} \approx 0.81$ m and $x_{sep} \approx 2$ m, respectively). Both experimenters had to overcome severe trouble with secondary flows, however.

Bearing in mind these experiments we intended to investigate three of the above-mentioned boundary-layer flows somewhat further. First a turbulent boundary layer with zero skin friction was generated where no three-dimensional effects could affect the flow, be it either from corner

flow or from secondary flow due to the geometry of the test section. Secondly the pressure gradient was adjusted such that the boundary layer separated, went through a region of reverse flow, and then reattached maintaining a flow with zero skin friction. Having set up flow configurations with separating and nearly separating boundary layers it seemed interesting to compare them with a more "normal" separation condition. This led to the third pressure distribution which had a region with nearly constant skin friction after a recovery from a sharp pressure rise and then approached separation.

Since boundary-layer separation is one of the limiting conditions of many applications of fluid mechanics the problem of a boundary layer with zero skin friction was recognized by Prandtl[11] in 1935 and solved theoretically for the laminar boundary layer. Several other papers have since investigated this type of flow (see v.Doenhoff and Tetervin[12], Walz[13], Stratford[14], Townsend[15], Eppler[16]) and a closed solution for both plane and axisymmetric flow was found by the first author[17, 18]. All of these theoretical approaches dealt with turbulent boundary layers on the verge of separation.

Due to the limited amount of time available this report had to be split into three parts, the first of which is presented here. It deals with the establishment of the flow configurations investigated, listing measurements of the mean velocity profiles in the boundary layer, of the pressure distribution, and of the wall shear stress. A second report will be printed next year describing fluctuation velocities, shear stress measurements, and the turbulence structure of the boundary layers. Lastly a theoretical report is in progress dealing with the calculation of turbulent boundary layers near separation and with enclosed regions of separation.

Phenomenological Description of the Experiments

The test section consisted of two concentric circular cylinders with the flow in the axial direction (see Fig. 1). The boundary layer was generated on the inner Plexiglas cylinder whereas the free surface of the outer porous cylinder could be covered up to control the mass flow and thereby the streamwise pressure distribution. The versatility of the apparatus already shown by Moses[7] and Goldberg[8] enabled three types of boundary layers close to separation to be set up. The governing factor for the adjustment of the pressure distribution was the skin friction measured with sublayer fences and a very sensitive feather probe serving as a means to visualize the behavior of the flow.

Boundary-Layer Flow I (Run I)

A steep pressure rise at the inlet to the test section enforced a separation velocity profile in the boundary layer. Further downstream the pressure gradient was modified to hold the boundary layer at the verge of separation without letting it separate.

For this part of the flow the sublayer fences indicated zero pressure difference, i.e. zero skin friction.

The feather probe hovered but did not show reverse flow on the wall.

Boundary-Layer Flow II (Run II)

A steeper pressure rise than the first one at the entry of the test section caused the boundary layer to separate. The sublayer fences and the feather probe indicated reverse flow. Downstream the pressure was adjusted in such a way to set up a reattaching boundary layer close to separation. Now the sublayer fences showed zero skin friction, except for a short region with positive skin friction until the flow separated again towards the end of the test section.

Boundary-Layer Flow III (Run III)

The third pressure distribution was intended to generate a boundary layer with distinctly positive but very small and constant skin friction which would finally separate normally. The skin-friction distribution actually obtained was slightly higher. This was due to the limitations of the apparatus. Since the fan speed could not be controlled surge conditions were approached and the boundary-layer flow consequently became oscillatory and unstable. These unfavorable conditions were avoided by accepting the slightly higher skin-friction distribution. After a steep rise the pressure distribution flatened off, causing the tailpipe effect known in internal-flow configurations. The skin friction rose slightly, but the following pressure rise then induced the boundary layer to separate.

2. EXPERIMENTAL APPARATUS AND TEST PROCEDURE

The wind tunnel and test section used were designed and described by Goldberg in an earlier report[8]. A brief description will be given, however, so that the following can be understood without complete knowledge of Goldberg's paper. The geometric details were not given in Goldber's paper. Since it proved to be a rather time-consuming and tiresome task to establish the pressure distribution investigated, we give a detailed account of the geometric parameters involved in Table 1 and Fig. 1 so that the experiments can be reproduced easily.

2.1 Apparatus

The description of the apparatus partly follows Goldberg. An axial-flow fan, rated at 27,300 m^3/h at 76,2 mm of water static, fitted with a radial inlet, supplies air to the system. Downstream of the fan are flow straightening vanes, a screen, motor fairing, and diffuser all of which serve the purpose of reducing losses and steadying the flow. The air which

leaves the diffuser enters an aluminum settling chamber 1.83 m in diameter and 3.05 m long. The settling chamber contains a honeycomb flow straightener, a center tube which is held in place by a vertically mounted airfoil strut, and an 86-mesh silk screen with approximately 46% free-flow area for reducing turbulence. The center tube provides support for the upstream end of the test section, as well as for the honeycomb. To prevent blower vibrations from reaching the settling chamber a flexible coupling, actually a piece of heavy fabric, is used to seal the gap between blower and diffuser (the diffuser being rigidly attached to the settling chamber). The flow leaving the settling chamber was accelerated to approximately 20 m/s by a 9 to 1 area contraction which further reduced the longitudinal velocity variations in the flow. The free-stream turbulence intensity measured at the exit of the contraction was approximately 0.2%.

The test boundary layer was grown on the central Plexiglas cylinder being 0.254 m in diameter and 1.83 m in length. The outer porous-metal cylinder had a length of 1.22 m and was 0.61 m in diameter and an adjustable end plate caused the annulus pressure to be greater than ambient. The flow diffusing out through the porous surface thus created an adverse pressure gradient. The pressure distribution could be adjusted as desired by controlling the flow through the porous cylinder, by adjusting the end plate and by opening the by-pass. Narrow cloth bands and larger pieces of transparent polythene sheets were fastened on the outer surface of the porous cylinder to control the outflow. The transparent cover allowed the flow to be observed and checked by means of a sensitive feather probe. Furthermore the outer cylinder had been provided with a longitudinal slot and guides for making boundary layer traverses.

With a boundary layer extending halfway or more into the annulus the flow angle had to be checked towards the edge of the boundary layer. This

was also accomplished by means of the feather probe.

2.2 Instrumentation

Insofar as the same instrumentation was used we may refer the reader to Goldberg's report for a more detailed description. The inner Plexiglas cylinder was fitted with static-pressure taps spaced 50.8 mm apart along a line parallel to the cylinder center line. The static-pressure taps were 0.635 mm in diameter and the static pressures were read on an inclined multi-tube manometer. Since the pressure distribution was used only as a first indication for the type of flow desired, the accuracy of such a manometer was sufficient.

A micrometer screw with 55 mm maximum travel was used to traverse a flattened total-head tube across the boundary layer. The outside height of the probe was 0.127 mm. The dynamic head - to determine the velocity in the boundary layer - was recorded by means of a micromanometer manufactured by R. Hellwig Co., Berlin/Germany. This micromanometer is a nulling instrument, i.e. before the measurement the meniscus is adjusted to zero and after the pressure is applied a vessel with methanol is raised or lowered by means of a micrometer screw until the instrument reads zero again. The difference in height is shown digitally and the accuracy of the manometer is $\pm$ 0.005 mm of the manometer liquid.

The same micromanometer was used to obtain the skin-friction readings. Wall shear stress was measured by means of a Preston tube with 1.27 mm outer diameter and a series of fixed sub-layer fences* located on the test cylinder along a line parallel to the row of static-pressure taps (see Fig. 2).

Each of the sublayer fences was machined out of a brass plug 4.77 mm in diameter, pressed into the Plexiglas cylinder and then ground flush with the

---

*The first reference in which such a skin-friction meter is described was given by D. N. Bushmarin and T. V. Andreieva[19].

surface on either side of the fence. The fences were approximately 0.254 mm thick and 0.152 mm high and pressure holes are placed in each plug on either side of the fence. As tests showed each fence, however, had to be calibrated separately.

We used the Preston tube for all skin-friction measurements where the boundary had not yet approached separation, and the sublayer fences where the flow was on the verge of separation or where flow reversal occurred. Since it was not possible with this experimental set up to calibrate the sublayer fences in both directions a negative pressure difference could be used only qualitatively as an indication for the strength of the back flow.

A zero-pressure reading of the sublayer fence was assumed to indicate a boundary layer on the verge of separation though the Preston tube still showed a small positive reading. A plot of the universal law where u_τ was obtained from the Preston-tube reading indicated, however, that the value for the skin friction must be too high and so the Preston-tube readings close to separation were assumed to be erroneous and not used. The behavior of the feather probe could be correlated with the reading of the sublayer fence, at least qualitatively, and confirmed the reading of the sublayer fence near separation. Two sublayer fences ($x = 0.768$ m) were calibrated against the Preston tube and for the calibration a flow with zero pressure gradient was set up. To ensure that calibration errors due to a circumferential variation of skin friction were excluded the Preston tube was put on top of the sublayer fence and removed for the fence reading (see Fig. 3).

The actual values for the wall shear stress were obtained from Patel's[20] calibration curve

$$y^* = 0.8287 - 0.1381\, x^* + 0.1437\, x^{*2} - 0.0060\, x^{*3} \qquad (2\text{-}1)$$

where $y^* \equiv \log_{10} \left(\frac{\tau_w d^2}{4\rho \nu^2}\right)$; $x^* \equiv \log_{10} \frac{\Delta p_{Pr.} d^2}{4\rho \nu^2}$

$\Delta p_{Pr.}$ is the pressure difference between the Preston tube and the static-pressure tap, ρ the density, ν the kinematic viscosity and d the diameter of the Preston tube.

The measuring position for skin friction and velocity profiles is also shown in Fig. 2. The result of the calibration is given in Fig. 4 for one fence. For all velocity profiles skin friction data were taken at the position of the velocity profile with respect to the x and z coordinates. If no variations in skin friction could be observed readings at the position of the sublayer fence were plotted, too.

2.3 Test Procedure

For all three runs the static-pressure and skin-friction distributions were measured first, then the velocity profiles were taken and lastly the skin friction was checked again. To ensure that the flattened Pitot probe did not measure at an angle of incidence to the flow we controlled the flow direction well beyond the edge of the boundary layer. The flow did not change its direction parallel to the cylinder axis - within the limits of observation - before it almost reached the porous cylinder. So only the outer part of the three last profiles in Run II may be affected by this divergence. The boundary-layer flow was checked for axisymmetry in the vicinity of the wall by means of the feather probe and by skin-friction measurements.

2.4 Data Reduction

One computer program was utilized in reducing the data and in evaluating the mean flow parameters from the pressure measurements. From this the values of displacement thickness, momentum thickness, energy thickness, and the two shape parameters of the velocity profile were calculated for both their

two-dimensional and axisymmetric definitions:

	Two-dimensional	Axisymmetric
Displacement thickness		
δ_1	$\int_0^\delta (1- \frac{u}{u_\delta})\, dy$	$\int_0^\delta (1- \frac{u}{u_\delta})(1 + \frac{y}{R})\, dy$
Momentum thickness		
δ_2	$\int_0^\delta \frac{u}{u_\delta} (1 - \frac{u}{u_\delta})\, dy$	$\int_0^\delta \frac{u}{u_\delta} (1 - \frac{u}{u_\delta})(1 + \frac{y}{R})\, dy$
Energy thickness		
δ_3	$\int_0^\delta \frac{u}{u_\delta}\left[1 - (\frac{u}{u_\delta})^2\right] dy$	$\int_0^\delta \frac{u}{u_\delta}\left[1 - (\frac{u}{u_\delta})^2\right](1 + \frac{y}{R})\, dy$
Shape parameters		
H_{12}	δ_1/δ_2	δ_1/δ_2
H_{32}	δ_3/δ_2	δ_3/δ_2

The radius of the Plexiglas cylinder R was 127 mm. The maximum difference between the axisymmetric and two-dimensional values of Re_{δ_2} and H_{12} was found to exceed the values given by Goldberg[8] which were, on average, 10% and 2% respectively. The maximum difference for each run is shown in the following table where the axisymmetric case is used as reference (= 100%):

	Re_{δ_2}	H_{12}
Run I	-20 %	+6 %
Run II	-33 %	+5 %
Run III	-29 %	+9 %

From this it is evident that the transverse-curvature effect is considerable and that the axisymmetric definitions have to be used to describe the boundary layer.

All the characteristic experimental data are given in tables 3 to 8 at the end of this report to facilitate comparisons or evaluation for other research workers. The pressure measurements for the velocity profiles were not corrected for either wall effects or turbulence in the boundary layer. A comparison with hot-wire measurements especially in the region close to the wall will be presented, however, in part two of this report.

An evaluation of the data of reference 10 which were taken under similar conditions showed that the difference between Pitot tube and hot wire measurements did not exceed -3% for H_{12} and +5% for δ_2 with the results from the Pitot measurement as the reference.

The skin-friction measurements were compared with the semi-empirical law of Ludwieg and Tillmann[21].

$$C_f = 0.246 \cdot 10^{-0.678\, H_{12}} \cdot Re_{\delta_2}^{-0.268} \qquad (2\text{-}2)$$

and with a modified skin-friction law (see reference[22]) where the skin friction is extrapolated towards zero, a minor shortcoming of eqn. (2-2). The modified law yields for the skin friction:

$$C_f = 0.0580 \left(\log \frac{8.05}{H_{12}^{1.818}}\right)^{1.705} \cdot Re_{\delta_2}^{-0.268} \qquad (2\text{-}3$$

3. EXPERIMENTAL RESULTS

3.1 General Remarks

For a presentation of the experimental results it was thought convenient to make a few general remarks first and then describe the different runs one by one.

The development of the boundary-layer flow as characterized by the velocity u_δ at the edge of the boundary layer, the Reynolds number Re_{δ_2}

based on the momentum thickness, the skin-friction coefficient C_f, and the shape parameter H_{12} is presented in one diagram for each run. This facilitates a survey on what is actually going on in the boundary layer. At all the positions where a velocity profile was measured the skin friction and the free-stream velocity were plotted from the profile measurements. The other u_δ and C_f values were taken from the control measurement. The momentum thickness and the shape parameter were determined from the measured velocity profiles. All values are shown as a function of the coordinate x in the streamwise direction. x is the distance along the cylinder starting from where the surface becomes parallel to the cylinder axis, i.e. 6.35 mm upstream from the first static-pressure tap.

The velocity data were presented in two ways. First u/u_δ was plotted versus y/δ_2 with the downstream position as a parameter and secondly u/u_τ was presented as a function of $\log \frac{y\, u_\tau}{\nu}$ to check whether the velocity profiles agree with the law of the wall. For a comparison with theory we used the universal law with the constants A = 5.75 and B = 5.1 given by Coles[23].

3.2 Boundary-Layer Flow I (Run I)

The characteristic boundary-layer values are shown in Fig. 5. With decreasing velocity in the free stream the boundary-layer thickness increases and the skin friction is gradually reduced until it reaches zero for x > 0.45 m. The velocity gradient is adjusted in such a way that the skin friction remains virtually zero as judged from the readings of the sublayer fences. Towards the end of the test section it is not possible to control the velocity distribution anymore and the boundary layer finally separates. This change in the flow close to the wall could very distinctly be seen from the behavior of the feather probe.

From semi-empirical skin friction laws and Stratford's measurements the shape parameter was expected to remain constant after the boundary layer had reached the state "on the verge of separation". As it turned out, however, the shape parameter H_{12} declined again having reached a maximum value of 2.84. A further rise downstream was observed before the flow finally separated. A similar behavior of the shape parameter H_{12} was found in reference 10 where $(H_{12})_{max}$ was 2.39 and subsequently fell to a smaller value rising again at the last measuring station.

Stratford's[9] separation profiles on the other hand reached maximum values of $H_{12} = 2.57$ remaining constant for the last 3.40 mm of his test section. The Reynolds-number range was about the same for the three experiments, lying between $1100 < Re_{\delta_2} < 12000$.

Looking at the velocity profiles (see Fig. 6) two groups can be clearly distinguished. One comprising the profiles 3 to 9 shows the well known behavior of velocity profiles in a turbulent boundary layer with an adverse pressure gradient, i.e. the region of velocity defect near the wall increases downstream. The second group includes those profiles labelled 11 to 19. It is interesting to note that 11 and 19 lie on the same curve close to the wall. Profile 13 shows the biggest defect which agrees with the maximum value of H_{12}. For all profiles of this group the sublayer fences indicated zero skin friction. Including the data of Stratford who claims zero skin friction between $2.32 < H_{12} < 2.57$ we can conclude therefore from experimental evidence that zero skin friction is reached if the shape parameter H_{12} lies within a range

$$2.27 < H_{12} < 2.84$$

for Reynolds numbers between 1100 and 12000.

This, however, means that the boundary layer in reference 10 falls

within this range with only one profile (H_{12} = 2.39 "B" condition, x = 130") which agrees well with the shape of profiles 11 and 19 near the wall as can be seen from Fig. 7. Beyond a value $H_{12} \approx 2.45$ of the shape parameter a region of constant velocity becomes more and more pronounced and extends further into the boundary layer (profiles 13 and 15). This finding seems to agree with some of Stratford's profiles (see ref. 9, Fig. 8) though the curves make it difficult to decide whether the velocity is constant or rises slightly in his experiments. It is certainly not sufficient to describe a velocity profile by H_{12} alone if the skin friction is zero and it is doubtful whether Re_{δ_2} adds much more information. This can be seen from Run III where profile 21 shows the same behavior as do 13 and 15 though the shape parameter is H_{12}= 2.45. Only the Reynolds number has twice the value of the profiles in Run I. Before one can draw any further conclusions it will be necessary to know the turbulence structure of the separation profiles, the knowledge of which may help to shed some more light on the rather somber state of the art.

If the velocity-profile data are plotted with u/u_τ versus log $(y\ u_\tau/\nu)$, using the measured skin-friction values, very good agreement with the universal law of the wall is obtained as can be seen from Fig. 8. Since all the other profiles had zero skin friction only the first four velocity profiles could be shown. Due to the steep pressure gradient the straight line in Fig. 8 is rather short and the curves start to deviate at a value of log $(u_\tau\ y/\nu) \approx 100$. A velocity profile with zero pressure gradient (x = 0.768 m) is plotted for comparison. It is not surprising therefore to find that both skin friction laws show good agreement with the measurements (see Fig. 9) up to separation. None of the existing skin friction laws takes account of a varying shape parameter at separation which would explain the discrepancy between theory and experiment in the separation region.

Lastly skin friction was measured in intervals of 6 mm along the circumference (-127 mm < Z < + 127 mm) at three stations (x = 0.210; 0.514; 0.921 m) and the value measured at each station was found to be constant.

3.3 Boundary-Layer Flow (Run II)

The second flow configuration (see Fig. 10) shows a sharp decline in velocity at the beginning of the test section so that the boundary-layer has separated before reaching 1/6 of the total length of the cylinder. A region of reversed flow where the sublayer fences indicate negative skin friction is then followed by reattachment of the boundary layer. Through most of this region of reattached flow the skin friction is again zero as it was in Run I but the velocity profiles show a distinctly different behavior. Having just about recovered from the reversed flow near the wall, the velocity defect is pronounced (see profile 13 in Fig. 11) by a relative minimum. This minimum moves towards the wall further downstream (profile 14) and finally vanishes (see profile 21). Despite of the relative minimum there is some resemblance between these velocity profiles and those (15 to 19) of Run I. If the velocity profiles are evaluated and measurements are compared with the semi-empirical skin-friction laws, poor agreement is found (see Fig. 12) since the shape parameter H_{12} is too low to yield zero skin friction. Three reasons may be given for this disagreement. First, the behavior of the feather probe indicated highly turbulent flow which could mean that the Pitot probes read too high, both away from and close to the wall. The same could hold for the sublayer fence which may be influenced by highly turbulent flow. Second, the laws for two-dimensional boundary layers may no longer be applicable to this special flow still recovering from back flow. Third, the boundary layer fills about 60% and more of the annulus downstream of x = 0.61 m. This may change the behavior of the boundary layer.

Compared with Run I where the boundary layer was tripped at about $x = 0.044$ m irregularities in natural transition are probably the reason for the variations in skin friction seen in Fig. 13. It is not surprising that these variations do not continue through the separation region downstream of which they have vanished completely.

Lastly a preliminary qualitative investigation of the region of separated flow was conducted by means of the feather probe. This showed that the separated region reached a hight of about 50 mm and a length of about 300 mm on the surface of the Plexiglas cylinder which would correspond to a very stable ring-shaped separation bubble. Hopefully more information will be obtained by the hot-wire measurements to confirm this hypothesis.

3.4 Boundary-Layer Flow III (Run III)

As may be recalled the third pressure distribution was set up to generate a boundary layer where the skin friction should be almost constant and small and where a velocity profile at separation could be obtained. This seemed necessary for a comparison with the profiles of Runs I and II conducted under more extreme conditions.

A gradual reduction of the velocity gradient in the free stream reduced the downward trend of the skin friction (see Fig. 14) and even reversed it. This rise in skin friction is probably due to the so-called tail-pipe effect known from internal-flow configurations where a region with pressure rise is followed by a region with zero pressure gradient. Since the velocity profiles thereby have to change shape - the velocity in the vicinity of the wall rises - skin friction is increased. Reducing the free stream velocity u_δ downstream furthermore causes the wall shear stress to fall rather sharply until separation is finally reached. The shape parameter H_{12} follows this pattern.

As for the velocity profiles (see Fig. 15) no anomalies could be observed, profile 7 being close to separation while a true separation profile only appears at position 21 .

Though we encountered the same type of profile in all the three runs the evidence that this is the separation profile is not conclusive until we know the order of magnitude of the fluctuating velocity components which may influence the reading given by the flattened Pitot probe. The meniscus of the manometer fluid was steady, however, thus showing no indication of oscillating flow.

All experimental results obtained can be explained satisfactorily except the plot of the universal semilogarithmic law of the velocity profiles which is shown in Fig. 16. Contrary to the good agreement between measurements and theory in Fig. 8 all the measured values for Run III were below the theoretical curve by as much as 15 %. This cannot be explained by inaccuracies of the measurements and so far no explanation for the discrepancy can be given. Several control measurements of both velocity and skin friction confirmed the original results.

4. DISCUSSION OF RESULTS

Neither Stratford nor Spangenberg et al. measured velocity profiles and skin friction together in turbulent boundary layers close to separation. Therefore it was one of the aims of this investigation to gather both these pieces of information. Since the new experimental results agreed neither in all parts with Stratford's experimental results nor with the semi-empirical laws for skin friction an interpretation should be made with great care. Good agreement was found between measurements and the two semi-empirical laws up to the point of separation (see Figs. 9 and 17). For both regions with skin friction zero (Runs I and II) the semi-empirical laws gave skin-

friction values which were too high. This was due to the development of the shape parameter H_{12} in axial direction. H_{12} declined after having reached a maximum value thus causing the skin friction to rise again whereas the sublayer fences still gave zero skin friction readings. Two reasons may be responsible for this discrepancy. Firstly, both the sublayer fence and the Pitot probe may have been affected by fluctuation velocities close to the wall causing the measurements - especially of the sublayer fence - to be slightly erroneous. This is quite possible in a region close to or at separation where the mean velocities are very small near the wall.

Secondly the skin friction laws in their present form can no longer be applied once separation has been approached.

Furthermore it is interesting to note that the experiments on boundary layers with zero skin friction disagree in two other points. Spangenberg's and the present experiments indicate a relative minimum for H_{12} in the region close to separation. In Stratford's experiment the shape factor H_{12} rose from a first plateau with H_{12} = const = 2.32 to a second plateau with H_{12} = const = 2.57 further downstream, indicating no decline of the shape parameter. Both regions were affected by secondary flow, however, which may serve as an explanation for the different behavior of the shape parameter, since no secondary flow was observed in the other two test sections.

Three types of separation velocity profiles were found in the three investigations. Stratford measured profiles which close to the wall followed a law $u \sim y^{1/2}$. This could not be confirmed by either of the three other experiments though Stratford's data can also be interpreted as having a region of almost constant velocity close to the wall. This would agree with the one group found in the present experiments (profiles 13 and 15 in Run I and profile 21 in Run III). The second group of profiles observed agrees with Spangenberg's separation profile as plotted in Fig. 7. No conclusive

explanation can be given yet for the existence of the two types of velocity profiles near separation but more definite answers are expected from the second part of the experimental investigation and the theoretical work.

Lastly it should be remarked that the experimental set up used was extremely well suited for experiments on boundary layers close to separation since the flow was absolutely steady. This is usually not the case in diffuser flow or in boundary layers near separation on airfoils. So at least the problem of separation in turbulent boundary layers for steady flows seems closer to a solution than before and might then make it possible to answer related questions for unsteady flows.

RECOMMENDATIONS FOR FURTHER RESEARCH

The second part of this investigation should be concerned with hot-wire measurements in the three turbulent boundary layers described above, following in general the procedure indicated in the paper of Spangenberg, Rowland, and Mease[10].

This would mean measuring the fluctuation velocities u' and v' as well as the shear stress distribution across the boundary layer. From these data the dissipation integral and the Reynolds - normal stress term - $\partial (\rho \overline{u'^2})/\partial x$ could be determined to check whether the latter term is as important as reference 10 indicates.

Furthermore it would be important to investigate the separated region found in Run II in more detail.

Lastly it would be necessary to estimate the influence of turbulent fluctuations near the wall on the reading of the sublayer fence.

REFERENCES

1. Bradshaw, P., Ferris, D. H., "The response of a retarded equilibrium turbulent boundary layer to the sudden removal of pressure gradient", 1965 N.P.L. Aero Rep. 1145.

2. Bradshaw, P., "The turbulence structure of equilibrium boundary layers", 1966 N.P.L. Aero Rep. 1184.

3. Herring, H. J., Norbury, J. F., "Some experiments on equilibrium turbulent boundary layers in favorable pressure gradients", J. Fluid Mech. 27 (1967), 541 - 549.

4. Schubauer, G. B., Spangenberg, W. G.,"Forced mixing in boundary layers", J. Fluid Mech. 8 (1960), 10-32.

5. Moses, H. L., Chappell, J. R., Goldberger, T., "Boundary layer separation in internal flow", M.I.T. Gas Turbine Laboratory (1965) Rep. 81.

6. Perry, A. E., "Turbulent boundary layers in decreasing adverse pressure gradients", J. Fluid Mech. 26 (1966), 481 - 506.

7. Moses, H. L., "The behavior of turbulent boundary layers in adverse pressure gradients", M.I.T. Gas Turbine Laboratory (1964), Rep. 73

8. Goldberg, P., "Upstream history and apparent stress in turbulent boundary layers", M.I.T. Gas Turbine Lab. (1966) Rep. 85.

9. Stratford, B. S., "An experimental flow with zero skin friction throughout its region of pressure rise", J. Fluid Mech. 5 (1959) pp 17 - 35.

10. Spangenberg, W. G., Rowland, W. R., Mease, N. E., "Measurements in a turbulent boundary layer maintained in a nearly separating condition" in *Fluid Mechanics of Internal Flow*, Editor G. Sovran, 1967, 110-151.

11. Prandtl, L., *Aerodynamic Theory*, Editor Durand, Vol. III, Berlin, 1934.

12. Doenhoff, A. E., Tetervin, N., "Determination of general relations for the behavior of turbulent boundary layers", NACA R 772, 1943.

13. Walz, A., "Theoretische Widerstandsberechnungen an einem Laminarprofil mit verschiedenen Schwanzteilformen (1944) Deutsche Luftfahrtforschung U & M 3131.

14. Stratford, B. S.,"The prediction of separation of the turbulent boundary layer", J. Fluid Mech. 5, 1959, pp 1 - 16.

15. Townsend, A. A., "The development of turbulent boundary layers with negligible wall stress", J. Fluid Mech. 8, 1960, 143 - 155.

16. Eppler, R., "Ergebnisse gemeinsamer Anwendung von Grenzschicht und Profiltheorie", Z. Flugwissenschaften 8, H.9, 1960.

17. Fernholz, H., "Theoretische Untersuchung zur optimalen Druckumsetzung in Unterschalldiffusoren", Dissertation, T.H. Karlsruhe, 1961.

18. Fernholz, H., "Eine grenzschichttheoretische Untersuchung optimaler Unterschalldiffusoren", Ingenieur Archiv 35, H. 3, pp 192-201, 1966.

19. Bushmarin, O. N., Andreieva, T. V., "Measuring friction in the turbulent boundary layer by Pitot tubes, A.R.C. 20,051 London B.S.R.A. Transl. No. 941 (1960).

20. Patel, V. C., "Calibration of the Preston tube and limitations on its use in pressure gradients", J. Fluid Mech. 23 (1965) pp 185-208.

21. Ludwieg, H., Tillmann, W., "Untersuchung ueber die Wandschubspannung in turbulenten Reibungsschichten, Ing. Archiv 17, 1949.

22. Fernholz, H., "Halbempirische Gesetze zur Berechnung turbulenter Grenzschichten nach der Methode der Integralbedingungen, Ing. Archiv 33 (1964), pp. 384 - 395.

23. Coles, D., "The law of the wake in the turbulent boundary layer", J. Fluid Mech. 1, (1956) pp 191-226.

TABLE 1 - GEOMETRIC VARIABLES IN MM

(For Reference See Figure 1)

VARIABLES	L_1	L_2^*	L_3	L_4^*	L_5	L_6^*	L_7	L_{01}	L_{10}	S_1	S_2	S_3	S_4
Run I	50.8	152.4	101.6	98.4	98.4	508.0	149.2	1828.8	635.0	12.7	12.7	12.7	76.2
Run II	254.0	736.6	47.6	120.65	-	-	-	1828.8	635.0	12.7	12.7	25.4	76.2
Run III	254.0	323.85	9.5	438.15	127.0	-	-	1828.8	635.0	12.7	12.7	15.87	76.2

TABLE 2 - CHARACTERISTIC BOUNDARY LAYER DATA (RUN I)

x[m]	u_∞[m/s]	$Re_x \times 10^{-5}$	u_τ[m/s]	τ_w[N/m^2]	c_f	δ_1[mm]	δ_2[mm]	δ_3[mm]	H_{12}	H_{32}	$Re_{\delta_2} \times 10^{-4}$
0.108	17.90	1.1993	0.8171	0.7764	0.00417	1.4561	1.0268	1.8054	1.4182	1.7583	0.1140
0.210	16.43	2.1364	0.6880	0.5501	0.00351	2.1023	1.4685	2.5568	1.4315	1.7411	0.1494
0.311	14.82	2.8539	0.5282	0.3242	0.00254	3.8839	2.5088	4.2730	1.5481	1.7032	0.2302
0.413	13.08	3.4606	0.3298	0.1289	0.00127	8.0882	4.2627	6.7878	1.8974	1.5923	0.3572
0.514	12.10	4.0438	≈0	≈0	≈0	17.540	7.1629	10.876	2.4488	1.5184	0.5635
0.616	11.44	4.5849	≈0	≈0	≈0	24.438	8.5990	12.885	2.8420	1.4985	0.6400
0.718	11.11	5.1069	≈0	≈0	≈0	26.112	10.172	15.446	2.5669	1.5185	0.7235
0.819	10.57	5.4964	≈0	≈0	≈0	28.603	12.585	19.425	2.2728	1.5435	0.8446
0.921	9.97	5.9898	≈0	≈0	≈0	37.534	15.973	24.592	2.3498	1.5396	1.0388
1.022	7.32	5.6882	-	negative	-	-	-	-	-	-	-

TABLE 3 - VELOCITY PROFILES (RUN I)

x = 0.108 m		x = 0.210 m		x = 0.311 m		x = 0.413 m		x = 0.514 m	
y/δ_2	u/u_δ	y/δ_2	u/u_δ	y/δ_2	u/u_δ	y/δ_2	u/u_δ	y/δ_2	u/u_δ
0.124	0.3173	0.09	0.3305	0.05	0.2203	0.0298	0.228	0.0177	0.149
0.247	0.4246	0.14	0.3999	0.10	0.2966	0.328	0.319	0.195	0.183
0.371	0.5069	0.23	0.4600	0.15	0.3629	0.625	0.371	0.372	0.199
0.485	0.5642	0.31	0.5068	0.20	0.3957	0.89	0.410	0.532	0.220
0.618	0.6090	0.40	0.5501	0.25	0.4252	1.13	0.450	0.71	0.230
0.741	0.6438	0.49	0.5785	0.30	0.4529	1.49	0.492	0.886	0.245
0.865	0.6628	0.57	0.5911	0.35	0.4738	1.79	0.541	1.063	0.266
0.990	0.6746	0.66	0.6006	0.40	0.4865	2.09	0.586	1.42	0.309
1.235	0.6984	0.75	0.6108	0.51	0.5006	2.38	0.632	1.77	0.388
1.482	0.7227	0.87	0.6314	0.61	0.5214	2.68	0.682	.213	0.454
1.978	0.7599	1.13	0.6573	0.81	0.5481	2.98	0.728	2.48	0.548
2.475	0.7880	1.47	0.6927	1.01	0.5740	3.28	0.772	2.66	0.580
4.950	0.9105	1.82	0.7240	1.27	0.6059	3.58	0.814	2.84	0.620
7.420	0.9775	2.59	0.7780	1.52	0.6352	4.05	0.856	3.01	0.655
9.900	0.9964	3.46	0.8360	2.02	0.6989	4.17	0.895	3.19	0.688
12.370	0.9984	4.32	0.8846	3.04	0.8039	4.77	0.955	3.37	0.727
19.790	1.00	5.19	0.9240	4.05	0.8916	5.36	.987	3.55	0.764
		6.05	0.9580	5.06	0.9540	5.66	.994	3.72	0.798
		6.92	0.9796	6.07	0.9822	5.96	1.00	3.90	0.836
		7.78	0.9891	7.09	0.9930	6.26	1.00	4.08	0.860
		8.65	0.9951	9.1.	0.9960			4.26	0.895
		10.38	0.9983	11.14	0.9970			4.43	0.922
		13.84	1.00	14.17	0.9979			4.61	0.943
				19.24	0.9988			4.79	0.959
				29.36	1.00			4.96	0.971
								5.14	0.984
								5.32	0.991
								5.50	0.996
								5.67	0.998
								5.85	1.00
								6.03	1.00

TABLE 3 - VELOCITY PROFILES (RUN I) (Continued)

x = 0.616 m		x = 0.718 m		x = 0.819 m		x = 0.921 m	
y/δ_2	u/u_δ	y/δ_2	u/u_δ	y/δ_2	u/u_δ	y/δ_2	u/u_δ
0.0148	0.122	0.013	0.126	0.010	0.114	0.00795	0.114
0.163	0.122	0.137	0.126	0.21	0.194	0.167	0.180
0.310	0.122	0.262	0.156	0.40	0.250	0.318	0.197
0.59	0.122	0.50	0.181	0.61	0.273	0.477	0.207
0.89	0.166	0.75	0.200	0.81	0.277	0.636	0.222
1.18	0.204	1.00	0.235	1.01	0.308	0.795	0.255
1.48	0.254	1.25	0.256	1.21	0.335	0.955	0.291
1.77	0.319	1.50	0.325	1.41	0.366	1.113	0.312
1.92	0.345	1.75	0.368	1.61	0.411	1.43	0.360
2.06	0.372	2.00	0.417	1.82	0.458	1.59	0.395
2.36	0.439	2.25	0.482	2.02	0.504	1.75	0.438
2.66	0.499	2.50	0.532	2.22	0.544	1.91	0.467
2.81	0.536	2.75	0.600	2.42	0.588	2.067	0.516
2.95	0.566	2.87	0.624	2.62	0.634	2.225	0.552
3.10	0.604	3.00	0.655	2.83	0.688	2.384	0.592
3.25	0.637	3.12	0.686	3.03	0.734	2.54	0.624
3.40	0.682	3.37	0.745	3.23	0.781	2.70	0.664
3.54	0.711	3.62	0.790	3.43	0.821	2.86	0.702
3.69	0.745	3.87	0.844	3.63	0.863	3.02	0.739
3.84	0.782	4.11	0.888	3.83	0.894	3.18	0.777
3.99	0.805	4.37	0.923	4.24	0.933	3.50	0.849
4.14	0.835	4.62	0.948	4.64	0.970	3.82	0.901
4.28	0.865	4.87	0.970	5.05	0.991	4.13	0.936
4.43	0.890	5.12	0.981	5.45	0.997	4.45	0.964
4.58	0.915	5.24	0.989	5.65	1.00	4.77	0.984
4.73	0.933	5.74	1.00			5.09	0.997
4.87	0.949	5.99	1.00			5.25	1.00
5.02	0.965					5.41	1.00
5.17	0.977						
5.32	0.990						
5.46	1.00						
5.61	1.00						

TABLE 4 - CHARACTERISTIC BOUNDARY LAYER DATA (RUN II)

x[m]	u_δ[m/s]	$Re_x \cdot 10^{-5}$	u_τ[m/s]	τ_w[N/m^2]	C_f	δ_1 [mm]	δ_2 [mm]	δ_3 [mm]	H_{12}	H_{32}	$Re_{\delta_2} \cdot 10^{-4}$
0.108	12.73	0.8701	0.4399	0.228	0.00239	3.6172	2.2040	3.6739	1.6412	1.6669	0.1776
0.159	11.27	1.1406	0.2133	0.0538	0.00072	9.5218	4.2873	6.6477	2.2209	1.5506	0.3076
0.616	8.94	3.4943	0	0	0	55.781	22.563	34.437	2.4722	1.5263	1.2799
0.667	8.82	3.7234	0	0	0	52.748	25.712	40.333	2.0515	1.5686	1.4353
0.717	8.71	3.9752	0	0	0	49.007	27.136	43.640	1.8060	1.6082	1.5045
0.819	8.35	4.4035	0	0	0	58.187	35.273	57.939	1.6496	1.6426	1.8965
0.921	7.79	4.5932	0	0	0	60.081	37.474	62.013	1.6033	1.6548	1.8689
1.022	7.15	4.6484	0	0	0	70.834	43.229	71.313	1.6386	1.6497	1.9662

TABLE 5 - VELOCITY PROFILES (RUN II)

x = 0.108 m		x = 0.159 m		x = 0.616 m		x = 0.667 m	
y/δ_2	u/u_δ	y/δ_2	u/u_δ	y/δ_2	u/u_δ	y/δ_2	u/u_δ
0.05	0.2110	0.030	0.1471	0.0056	0.232	0.005	0.2361
0.346	0.400	0.326	0.2225	0.062	0.256	0.054	0.3184
0.634	0.472	0.620	0.2589	0.118	0.280	0.104	0.3184
0.92	0.517	0.918	0.2960	0.225	0.262	0.148	0.3184
1.21	0.558	1.185	0.3443	0.34	0.249	0.198	0.3103
1.49	0.597	1.481	0.3997	0.45	0.210	0.296	0.3103
1.729	0.629	1.777	0.4541	0.56	0.210	0.397	0.2906
2.017	0.662	2.073	0.5127	0.68	0.198	0.494	0.2906
2.304	0.692	2.370	0.5653	0.79	0.206	0.593	0.2906
2.881	0.756	2.660	0.6218	0.90	0.181	0.692	0.2992
3.457	0.817	2.962	0.6811	1.01	0.218	0.79	0.3130
4.034	0.865	3.258	0.7286	1.13	0.225	0.89	0.3262
4.609	0.911	3.555	0.7733	1.24	0.245	0.99	0.3463
5.186	0.948	3.851	0.8249	1.35	0.271	1.19	0.3855
5.762	0.971	4.147	0.8675	1.46	0.297	1.383	0.4271
6.339	0.986	4.443	0.9082	1.58	0.346	1.58	0.4740
6.915	0.996	4.740	0.9443	1.80	0.425	1.78	0.5295
7.491	1.00	5.036	0.9659	1.91	0.447	1.88	0.5560
		5.332	0.9765	2.14	0.528	1.98	0.5812
		5.480	0.9870	2.36	0.589	2.27	0.6691
		5.924	0.9948	2.59	0.665	2.57	0.7466
		6.40	1.00	2.81	0.738	2.86	0.8012
				3.04	0.768	3.16	0.8670
				3.26	0.820	3.36	0.8910
				3.50	0.878	3.66	0.9282
				3.71	0.905	3.95	0.9639
				3.94	0.932	4.15	0.9769
				4.17	0.958	4.25	0.9830
				4.39	0.975	4.35	0.9872
				4.62	0.992	4.45	0.9915
				4.84	1.00	4.54	0.9958
						4.64	1.00

TABLE 5 CONTINUED - VELOCITY PROFILES (RUN II)

x = 0.717 m		x = 0.819 m		x = 0.921 m		x = 1.022 m	
y/δ_2	u/u_δ	y/δ_2	u/u_δ	y/δ_2	u/u_δ	y/δ_2	u/u_δ
0.0047	0.238	0.004	0.229	0.003	0.186	0.003	0.2374
0.051	0.360	0.039	0.398	0.038	0.369	0.032	0.3162
0.094	0.371	0.076	0.426	0.071	0.413	0.061	0.3241
0.140	0.385	0.144	0.439	0.137	0.460	0.118	0.3685
0.187	0.385	0.288	0.462	0.274	0.487	0.235	0.4113
0.234	0.385	0.432	0.475	0.410	0.498	0.352	0.4442
0.281	0.387	0.576	0.479	0.545	0.505	0.470	0.4749
0.374	0.392	0.720	0.483	0.684	0.515	0.587	0.4803
0.468	0.392	0.864	0.497	0.81	0.534	0.705	0.5113
0.562	0.392	1.008	0.510	0.95	0.550	0.822	0.5310
0.655	0.398	1.152	0.538	1.08	0.556	0.940	0.5429
0.749	0.413	1.296	0.564	1.22	0.569	1.058	0.5569
0.842	0.415	1.368	0.575	1.29	0.580	1.116	0.5638
1.030	0.443	1.440	0.580	1.36	0.597	1.175	0.5728
1.217	0.473	1.584	0.604	1.49	0.611	1.292	0.5905
1.404	0.503	1.728	0.626	1.63	0.630	1.410	0.6096
1.591	0.546	1.872	0.656	1.76	0.654	1.527	0.6283
1.778	0.596	2.016	0.690	1.90	0.673	1.645	0.6464
1.965	0.631	2.160	0.717	2.03	0.694	1.763	0.6717
2.153	0.689	2.304	0.749	2.17	0.720	1.880	0.6886
2.340	0.724	2.448	0.773	2.30	0.745	1.998	0.7088
2.527	0.760	2.592	0.797	2.44	0.771	2.115	0.7267
2.714	0.795	2.736	0.824	2.58	0.791	2.233	0.7459
2.901	0.827	2.880	0.848	2.71	0.813	2.350	0.7679
3.089	0.871	3.024	0.880	2.85	0.842	2.468	0.7877
3.276	0.900	3.168	0.907	2.98	0.869	2.585	0.8069
3.557	0.928	3.312	0.927	3.12	0.900	2.703	0.8289
3.744	0.947	3.456	0.944	3.25	0.924	2.820	0.8488
3.931	0.963	3.600	0.962	3.39	0.943	2.938	0.8697
4.118	0.983	3.673	0.970	3.52	0.960	3.055	0.8986
4.306	0.991	3.816	0.978	3.66	0.976	3.173	0.9198
4.493	1.00	3.888	0.986	3.73	0.984	3.290	0.9405
		3.960	0.992	3.80	0.992	3.349	0.9513
		4.104	1.00	3.86	0.997	3.408	0.9607
				3.93	1.00	3.467	0.9713
						3.525	0.9779
						3.643	0.9935
						3.702	1.00

TABLE 6 - CHARACTERISTIC BOUNDARY LAYER DATA (RUN III)

x[m]	u_δ[m/s]	$Re_x \cdot 10^{-5}$	u_τ[m/s]	τ_w[N/m^2]	C_f	δ_1 [mm]	δ_2 [mm]	δ_3 [mm]	H_{12}	H_{32}	$Re_{\delta_2} \cdot 10^{-4}$	ν [m^2/s]$\cdot 10^4$
0.1080	14.58	0.9885	0.6020	0.4255	0.00341	2.0335	1.3345	2.2829	1.5238	1.7106	0.1221	0.1593
0.210	12.16	1.599	0.3538	0.1466	0.00169	5.2576	2.8701	4.6297	1.8318	1.6130	0.2185	0.1597
0.3112	10.91	2.137	0.2648	0.0825	0.00118	9.5594	4.6848	7.3474	2.0405	1.5684	0.3217	0.1589
0.4128	10.44	2.682	0.2954	0.1015	0.00160	10.760	5.9036	9.4861	1.8227	1.6068	0.3836	0.1607
0.5144	9.92	3.131	0.2876	0.0954	0.00168	11.960	6.7456	10.914	1.7729	1.6179	0.4106	0.1630
0.6160	9.69	3.655	0.2922	0.0983	0.00182	13.756	8.1137	13.321	1.6954	1.6418	0.4814	0.1633
0.7176	9.21	4.103	0.2981	1.032	0.00210	14.119	8.7251	14.517	1.6182	1.6638	0.4989	0.1611
0.8192	9.17	4.683	0.2860	0.0951	0.00194	17.817	11.057	18.389	1.6115	1.6632	0.6321	0.1604
0.9208	8.56	4.914	0.2182	0.0554	0.00130	27.170	15.104	24.466	1.7988	1.6198	0.8060	0.1604
1.0224	7.94	5.077	0	≈ 0	0	67.715	27.639	41.630	2.45	1.5424	1.3725	0.1599

TABLE 7 - VELOCITY PROFILES (RUN III)

x = 0.1080 m		x = 0.210 m		x = 0.311 m		x = 0.413 m		x = 0.514	
y/δ_2	u/u_δ	y/δ_2	u/u_δ	y/δ_2	u/u_δ	y/δ_2	u/u_δ	y/δ_2	u/u_δ
0.0955	0.2425	0.044	0.1766	0.027	0.1410	0.022	0.2095	0.0188	0.1844
0.324	0.3606	0.221	0.2705	0.135	0.2101	0.043	0.2316	0.094	0.2974
0.571	0.5100	0.398	0.3535	0.244	0.2679	0.065	0.249	0.170	0.3499
0.800	0.5718	0.575	0.3929	0.352	0.2934	0.086	0.2705	0.245	0.3689
1.050	0.6070	0.752	0.4150	0.461	0.3063	0.108	0.2901	0.320	0.3780
1.520	0.6584	0.930	0.4360	0.570	0.3221	0.129	0.306	0.396	0.3956
2.05	0.7016	1.15	0.4676	0.705	0.3420	0.150	0.322	0.47	0.4124
2.85	0.7810	1.33	0.5043	0.814	0.3532	0.193	0.340	0.56	0.4206
3.81	0.8512	1.55	0.5345	0.950	0.3685	0.236	0.347	0.75	0.4364
4.76	0.9024	1.77	0.5653	1.08	0.3860	0.280	0.347	0.94	0.4592
5.71	0.9475	2.21	0.6252	1.36	0.4268	0.366	0.366	1.13	0.4809
6.66	0.9781	2.65	0.6910	1.63	0.4722	0.451	0.389	1.32	0.5084
7.61	0.9953	3.10	0.7535	1.90	0.5147	0.667	0.406	1.51	0.5345
8.09	0.9985	3.54	0.8089	2.17	0.5529	0.86	0.428	1.88	0.5867
8.56	1.00	3.98	0.8634	2.44	0.6081	1.29	0.485	2.26	0.6442
		4.42	0.9068	2.71	0.6561	1.72	0.535	2.64	0.7047
		4.87	0.9424	2.98	0.7048	2.15	0.617	3.01	0.7586
		5.31	0.9737	3.25	0.7503	2.58	0.685	3.39	0.8123
		5.53	0.9796	3.52	0.8015	3.01	0.746	3.77	0.8650
		5.75	0.9846	3.80	0.8405	3.44	0.8226	4.14	0.9147
		5.97	0.9887	4.07	0.8790	3.87	0.875	4.71	0.9619
		6.19	0.9928	4.34	0.9147	4.30	0.927	5.08	0.9759
		6.42	0.9959	4.61	0.9397	4.73	0.956	5.46	0.9877
		6.64	0.9977	4.88	0.9646	5.16	0.978	5.84	0.9952
		7.08	1.00	5.15	0.9811	5.59	0.9908	6.21	0.9986
				5.42	0.9872	6.02	0.9957	6.40	1.00
				5.69	0.9917	6.45	0.9982		
				5.96	0.9956	7.31	1.00		
				6.24	0.9989				
				6.51	1.00				

TABLE 7 CONTINUED - VELOCITY PROFILES (RUN III)

x = 0.616 m		x = 0.718 m		x = 0.819 m		x = 0.921 m		x = 1.022 m	
y/δ_2	u/u_δ	y/δ_2	u/u_δ	y/δ_2	u/u_δ	y/δ_2	u/u_δ	y/δ_2	u/u_δ
0.016	0.1773	0.014	0.1900	0.0115	0.1733	0.008	0.1347	0.005	0.1522
0.078	0.2803	0.044	0.1900	0.0230	0.1906	0.017	0.1650	0.014	0.1654
0.141	0.3586	0.073	0.2628	0.0345	0.2065	0.025	0.1905	0.023	0.1777
0.204	0.3780	0.102	0.3362	0.0460	0.2576	0.042	0.2214	0.032	0.1892
0.266	0.3964	0.131	0.3717	0.0575	0.2948	0.059	0.2410	0.041	0.1892
0.329	0.4106	0.160	0.4002	0.0805	0.3325	0.076	0.2591	0.060	0.1892
0.407	0.4226	0.189	0.4118	0.1035	0.3729	0.092	0.2761	0.078	0.1892
0.470	0.4309	0.248	0.4286	0.127	0.3874	0.110	0.2889	0.097	0.1892
0.63	0.4472	0.306	0.4483	0.149	0.4014	0.143	0.2952	0.143	0.1892
0.78	0.4736	0.437	0.4771	0.195	0.4206	0.177	0.3072	0.184	0.1892
0.94	0.4928	0.582	0.4933	0.241	0.4318	0.261	0.3327	0.276	0.1892
1.25	0.5345	0.728	0.5089	0.299	0.4479	0.337	0.3539	0.368	0.1892
1.57	0.5732	0.873	0.5256	0.356	0.4618	0.50	0.3858	0.460	0.1892
1.88	0.6217	1.164	0.5533	0.4595	0.4736	0.67	0.4196	0.55	0.1892
2.19	0.6655	1.455	0.5917	0.6892	0.5059	0.84	0.4468	0.74	0.1892
2.50	0.7071	1.747	0.6277	0.9189	0.5406	1.01	0.4686	0.92	0.2052
2.82	0.7512	2.038	0.6606	1.148	0.5621	1.18	0.4931	1.10	0.2384
3.13	0.7955	2.329	0.7032	1.378	0.5868	1.35	0.5218	1.29	0.3244
3.44	0.8367	2.620	0.7359	1.608	0.6132	1.51	0.5472	1.47	0.3784
3.76	0.8799	2.911	0.7764	1.838	0.6384	1.68	0.5731	1.65	0.4255
4.07	0.9103	3.202	0.8120	2.067	0.6627	1.85	0.6159	1.75	0.4472
4.38	0.9373	3.493	0.8461	2.297	0.6884	2.02	0.6376	1.93	0.4920
4.70	0.9562	3.784	0.8788	2.527	0.7275	2.35	0.6896	2.11	0.5525
5.01	0.9710	4.075	0.9078	2.757	0.7645	2.69	0.7416	2.30	0.6035
5.32	0.9820	4.367	0.9326	2.986	0.7949	3.03	0.8083	2.48	0.6569
5.63	0.9892	4.658	0.9534	3.216	0.8242	3.20	0.8326	2.67	0.7108
5.95	0.9957	4.949	0.9689	3.446	0.8525	3.53	0.8762	2.85	0.7678
6.26	0.9979	5.240	0.9786	3.675	0.8798	3.87	0.9187	3.03	0.8131
6.57	1.00	5.531	0.9874	4.135	0.9253	4.04	0.9372	3.12	0.8373
		5.822	0.9937	4.594	0.9605	4.37	0.9620	3.40	0.8885
		6.404	0.9992	5.054	0.9792	4.54	0.9724	3.68	0.9325
		6.696	1.00	5.513	0.9921	4.88	0.9872	3.86	0.9459
				5.973	0.9984	5.21	0.9936	3.95	0.9537
				6.202	1.00	5.72	1.00	4.04	0.9614
								4.69	0.9862
								4.96	1.00

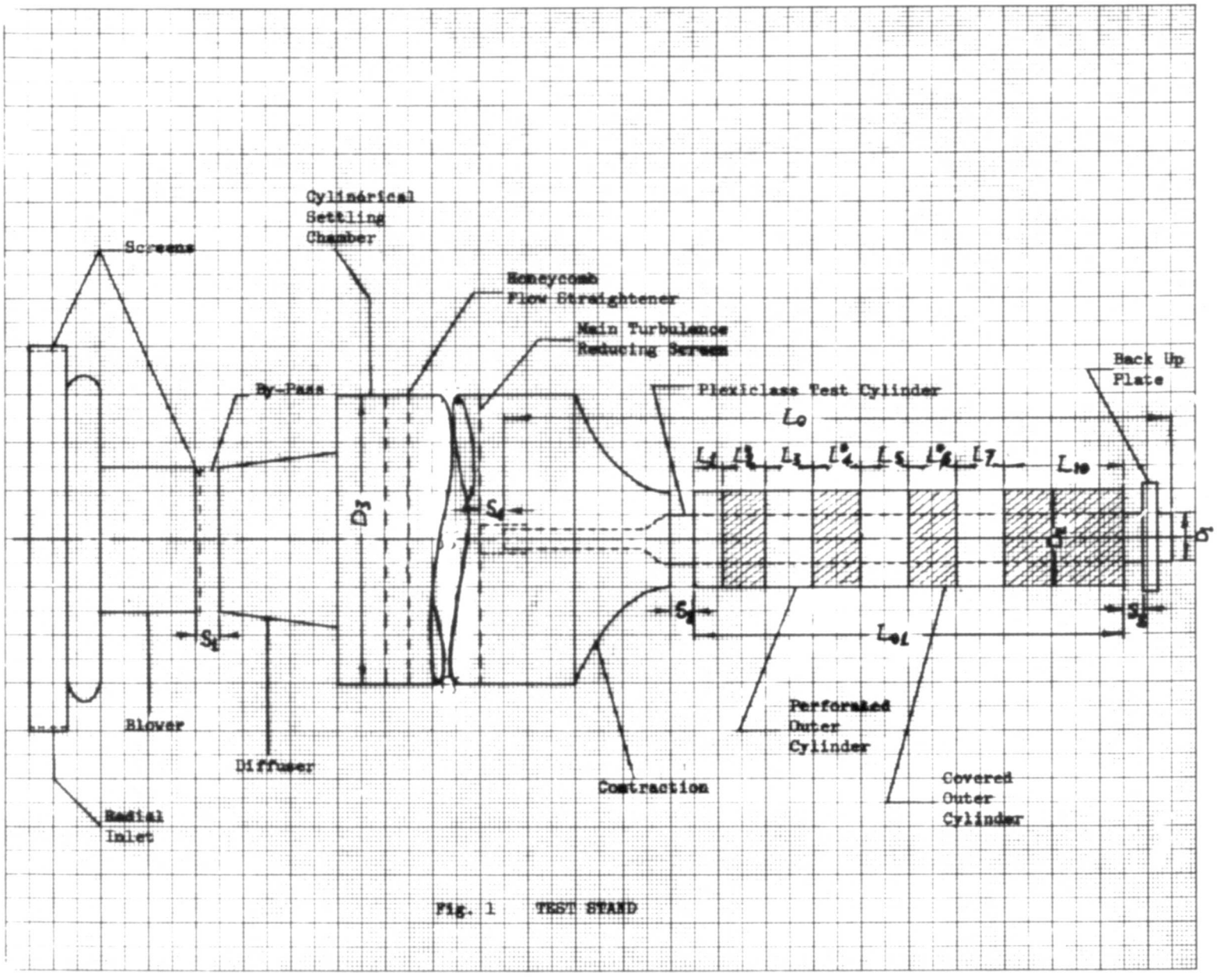

Fig. 1 TEST STAND

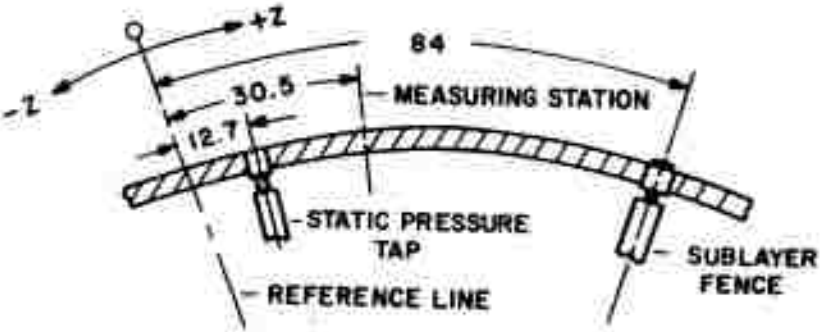
+Z
-Z
84
30.5
MEASURING STATION
12.7
STATIC PRESSURE TAP
REFERENCE LINE
SUBLAYER FENCE

FIG. 2

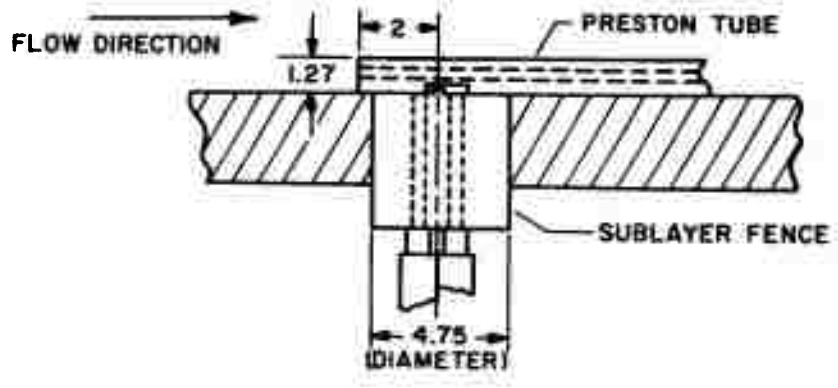

FIG. 3 EXPERIMENTAL SET-UP FOR SUBLAYER-FENCE CALIBRATION
(DIMENSIONS IN MM)

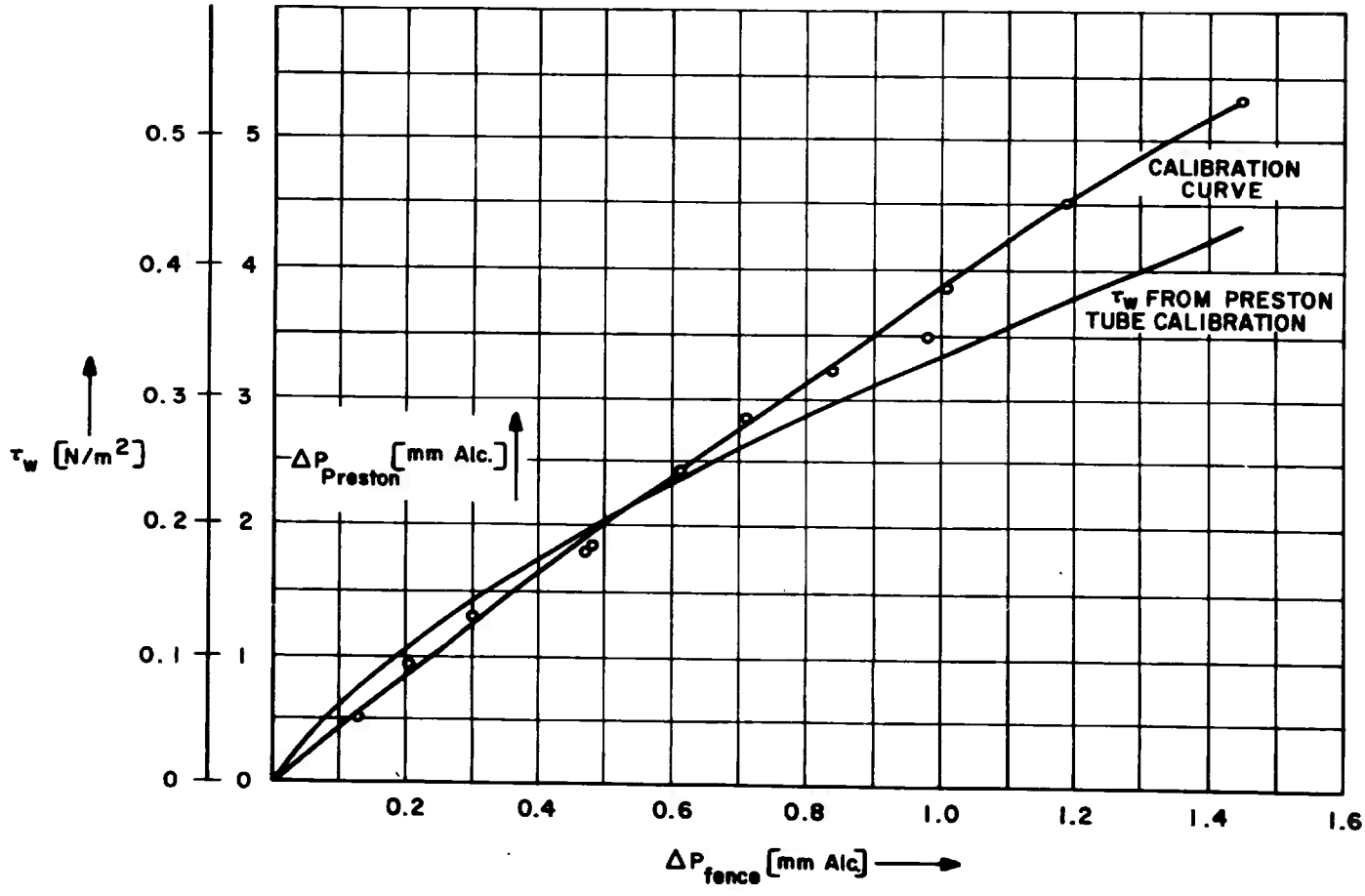

FIG. 4. CALIBRATION CURVE FOR THE SUBLAYER-FENCE AT X= 0.768 m

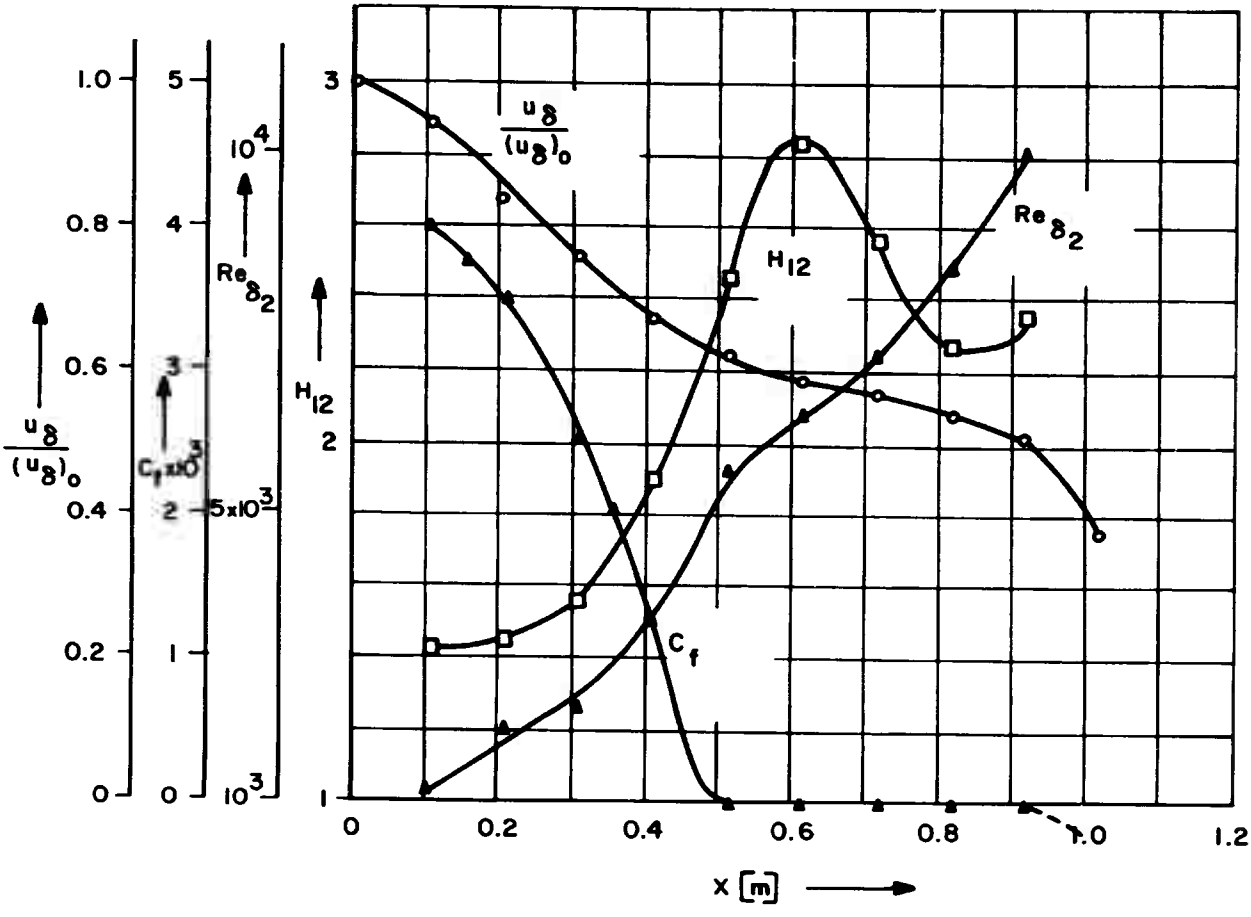

FIG. 5 REYNOLDS NUMBER, VELOCITY, SKIN FRICTION, AND H_{12} DISTRIBUTIONS (RUN I)

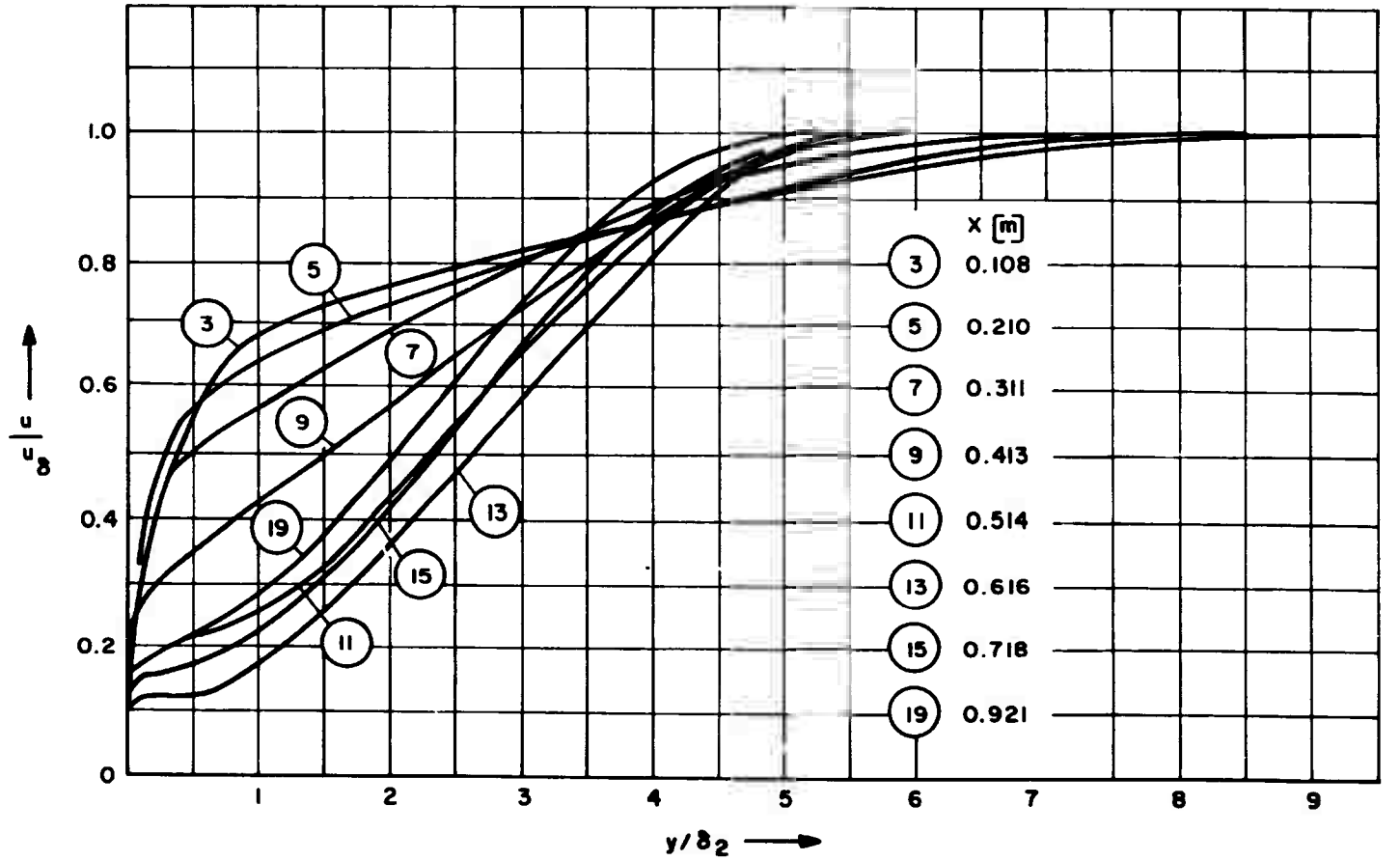

FIG. 6 VELOCITY PROFILES IN A TURBULENT BOUNDARY LAYER (RUN I)

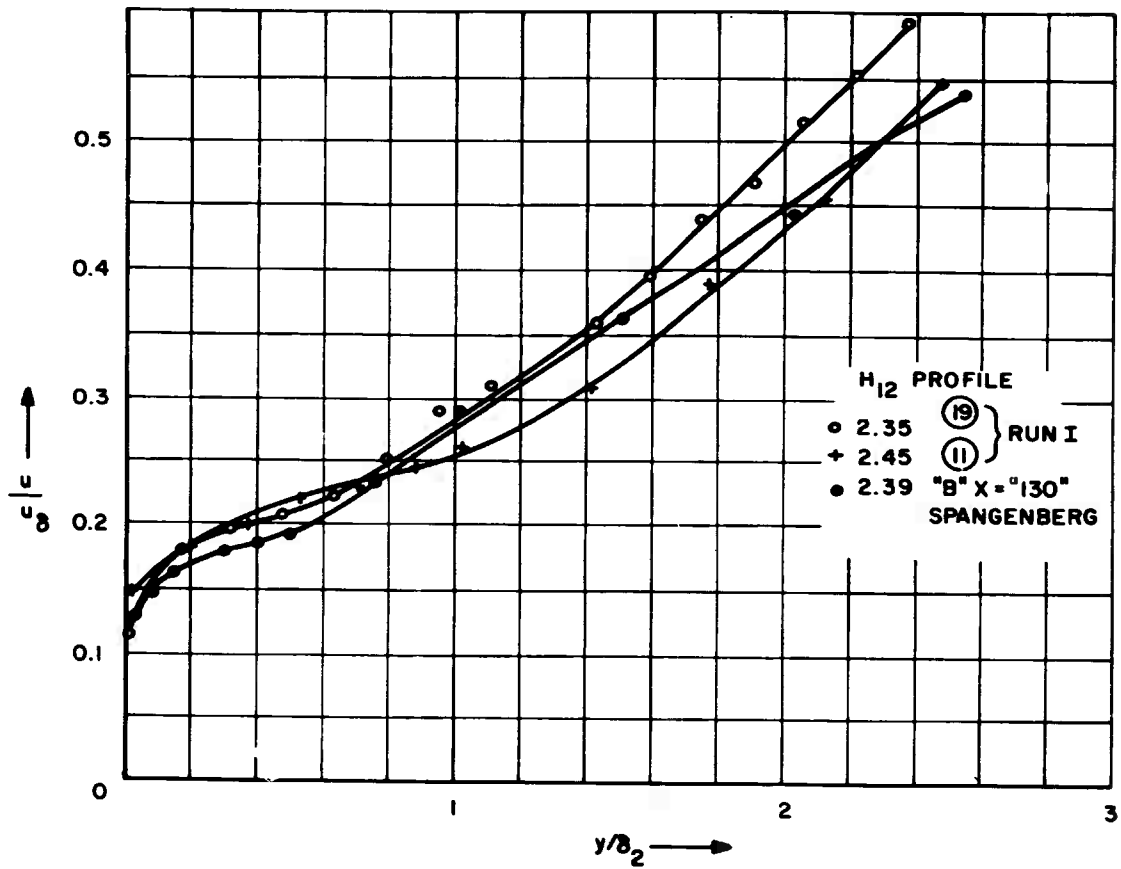

FIG. 7 SEPARATION PROFILES NEAR THE WALL IN A TURBULENT BOUNDARY LAYER

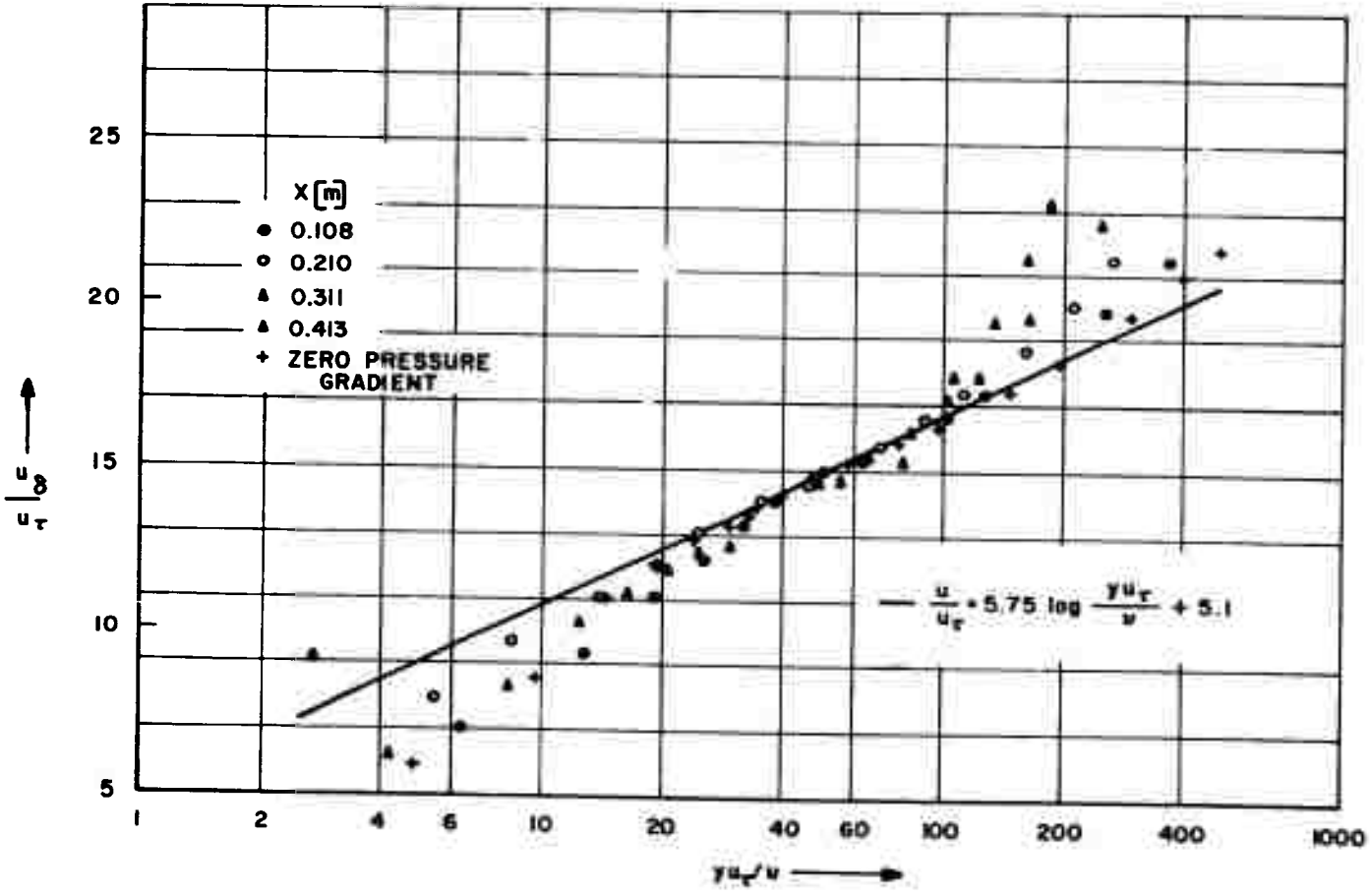

FIG. 8 UNIVERSAL SEMILOGARITHMIC LAW OF VELOCITY PROFILES (RUN I)

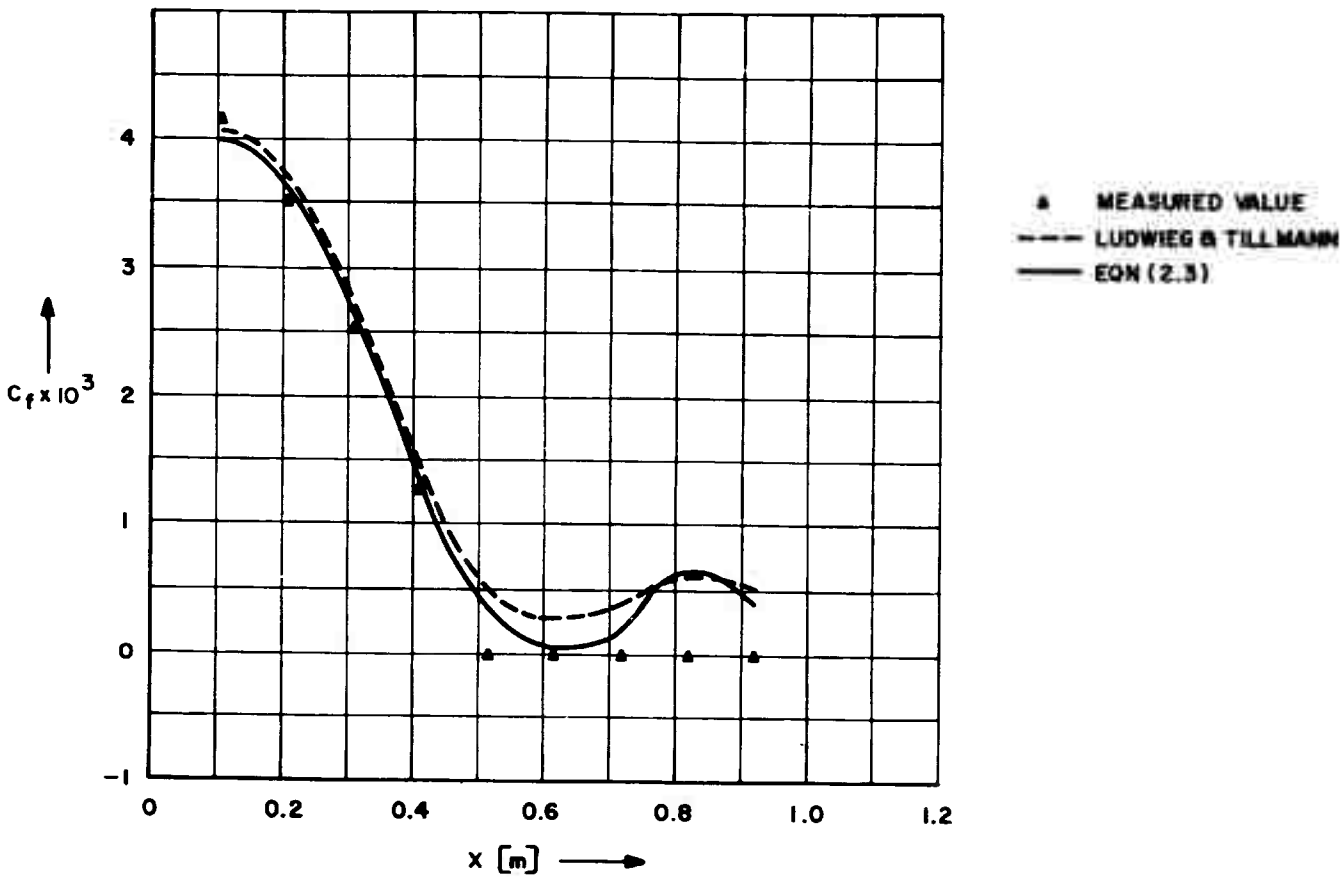

FIG. 9 EXPERIMENTAL AND THEORETICAL WALL SHEAR STRESS (RUN I)

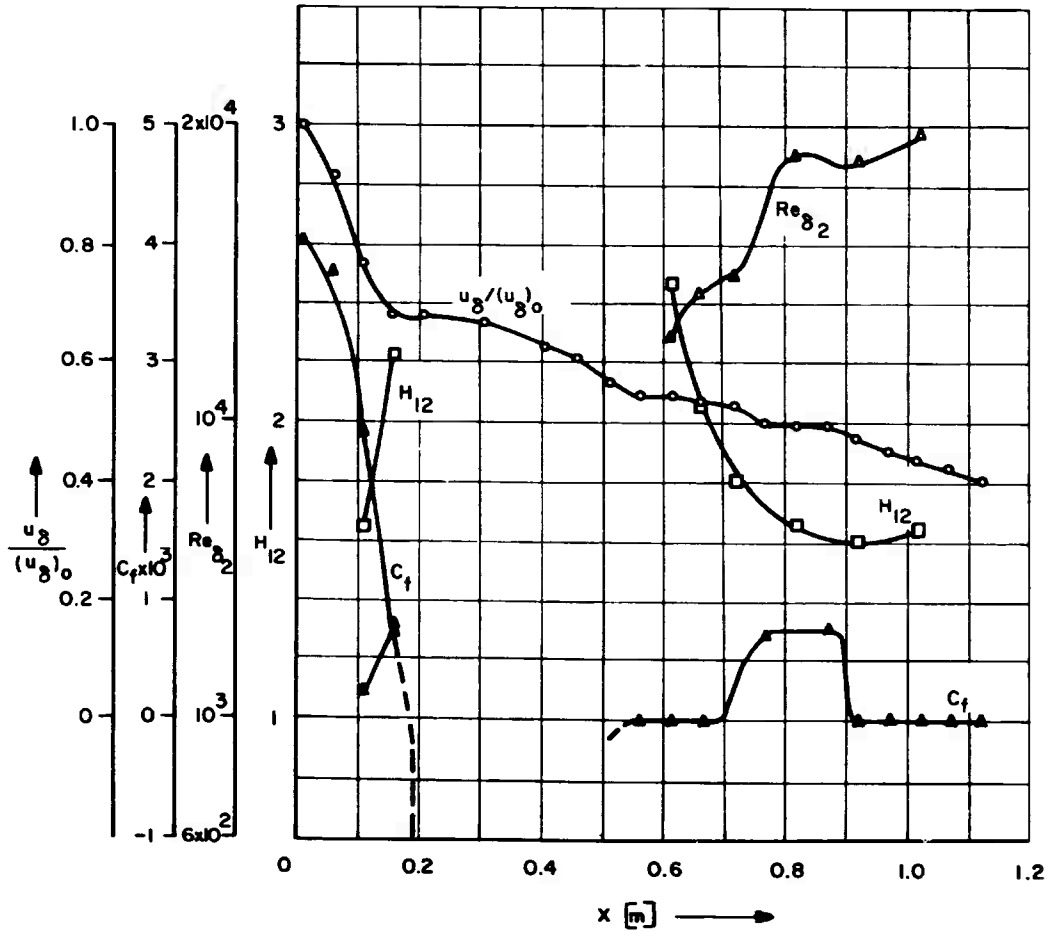

FIG. 10 REYNOLDS NUMBER, VELOCITY, SKIN FRICTION, AND H_{12} DISTRIBUTIONS (RUN II)

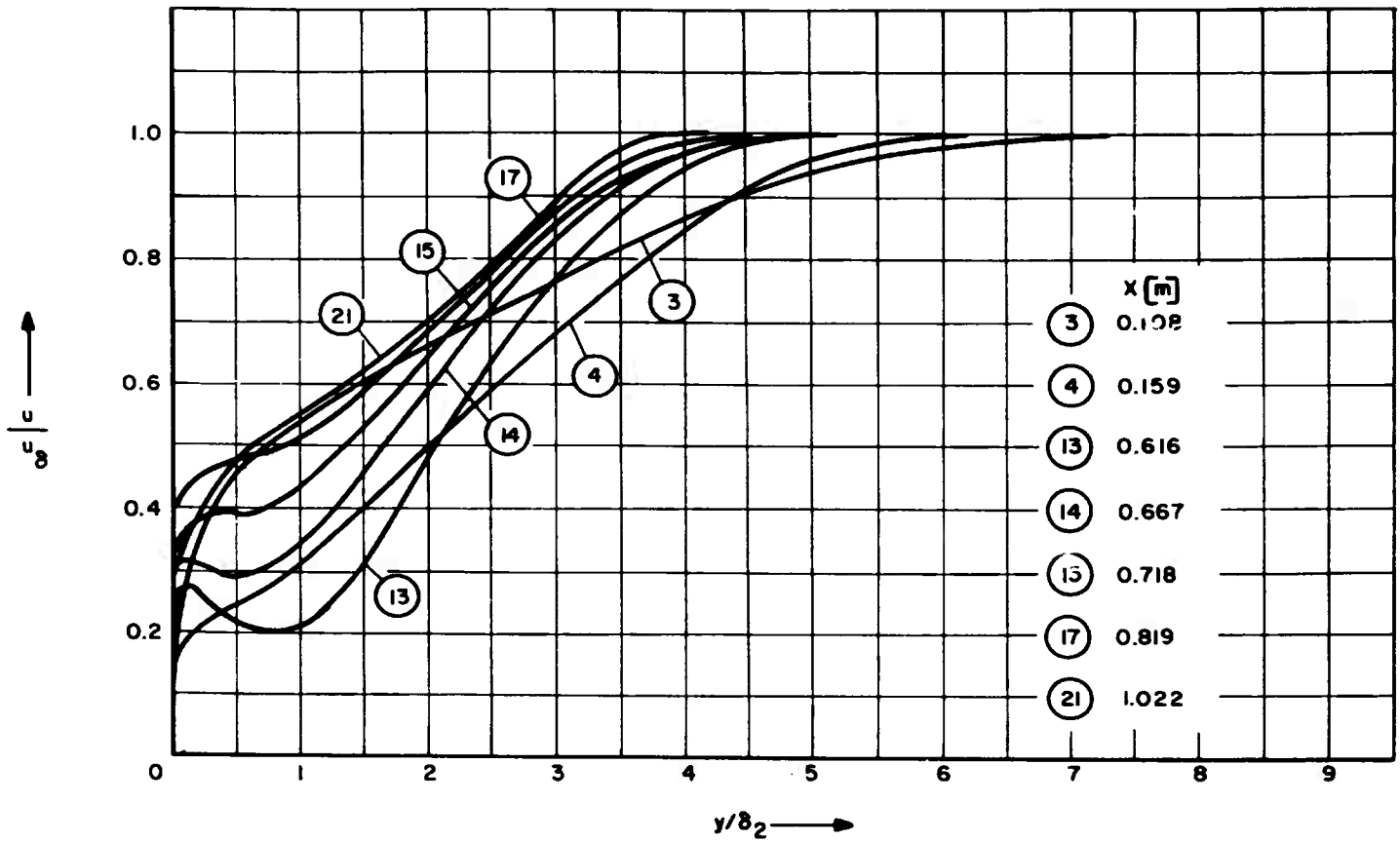

FIG. 11 VELOCITY PROFILES IN A TURBULENT BOUNDARY LAYER (RUN II)

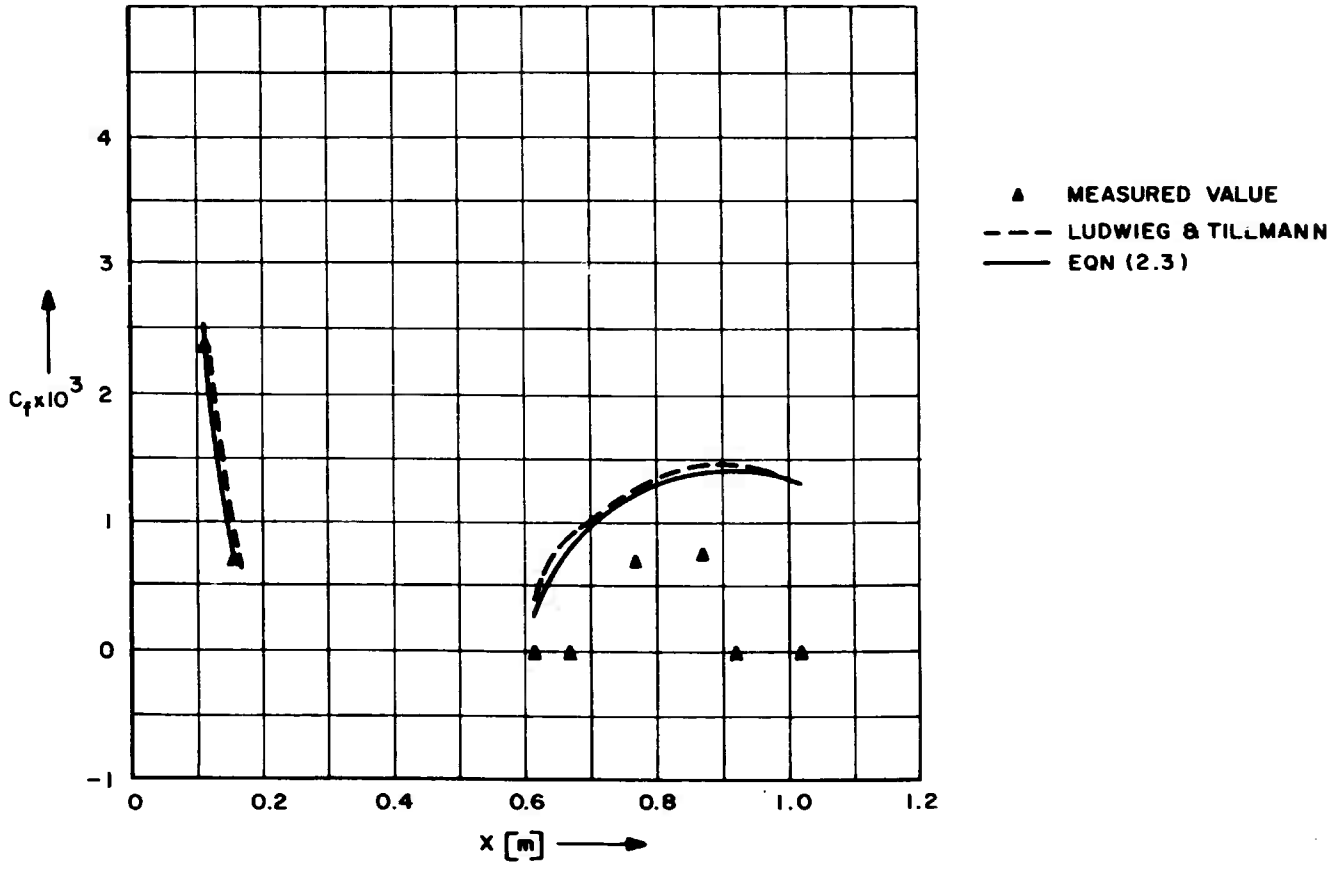

FIG. 12 EXPERIMENTAL AND THEORETICAL WALL SHEAR STRESS (RUN II)

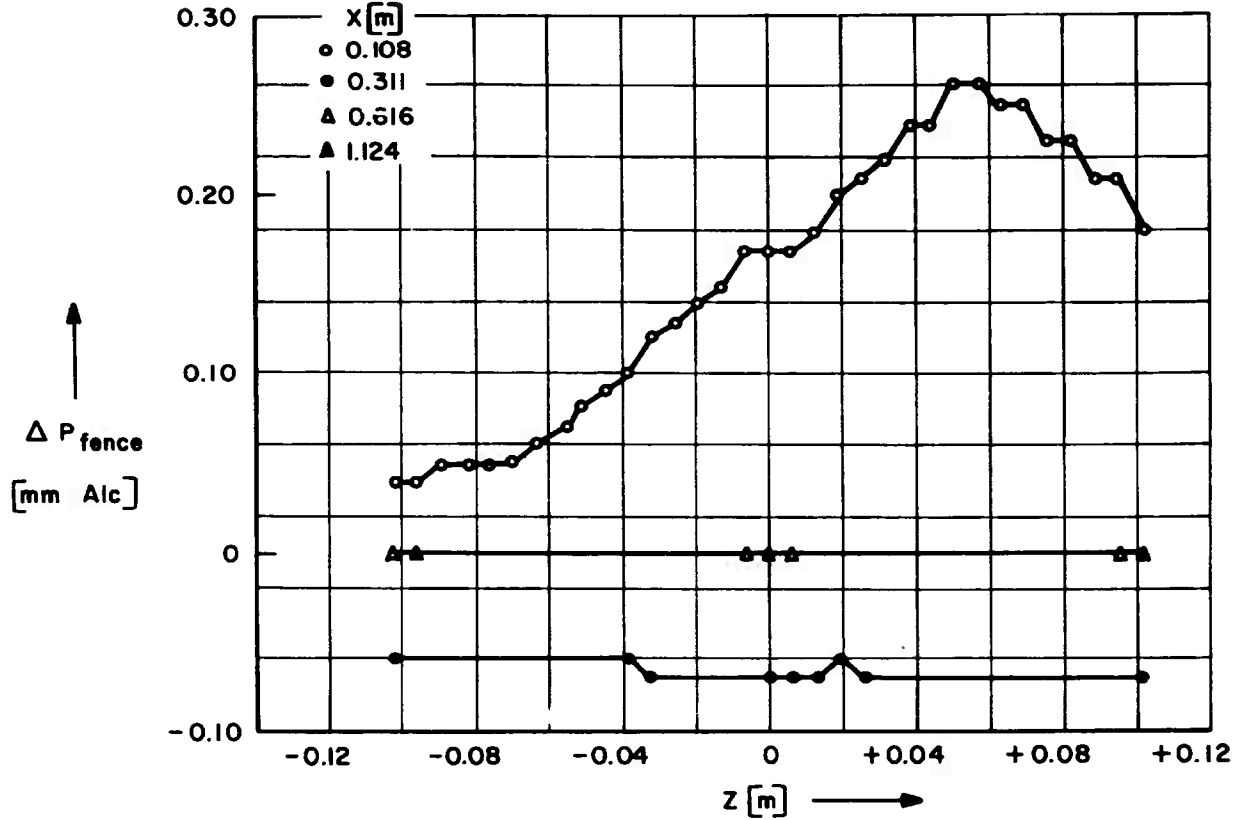

FIG.13 SKIN FRICTION DISTRIBUTION ALONG CIRCUMFERENCE (RUNII)

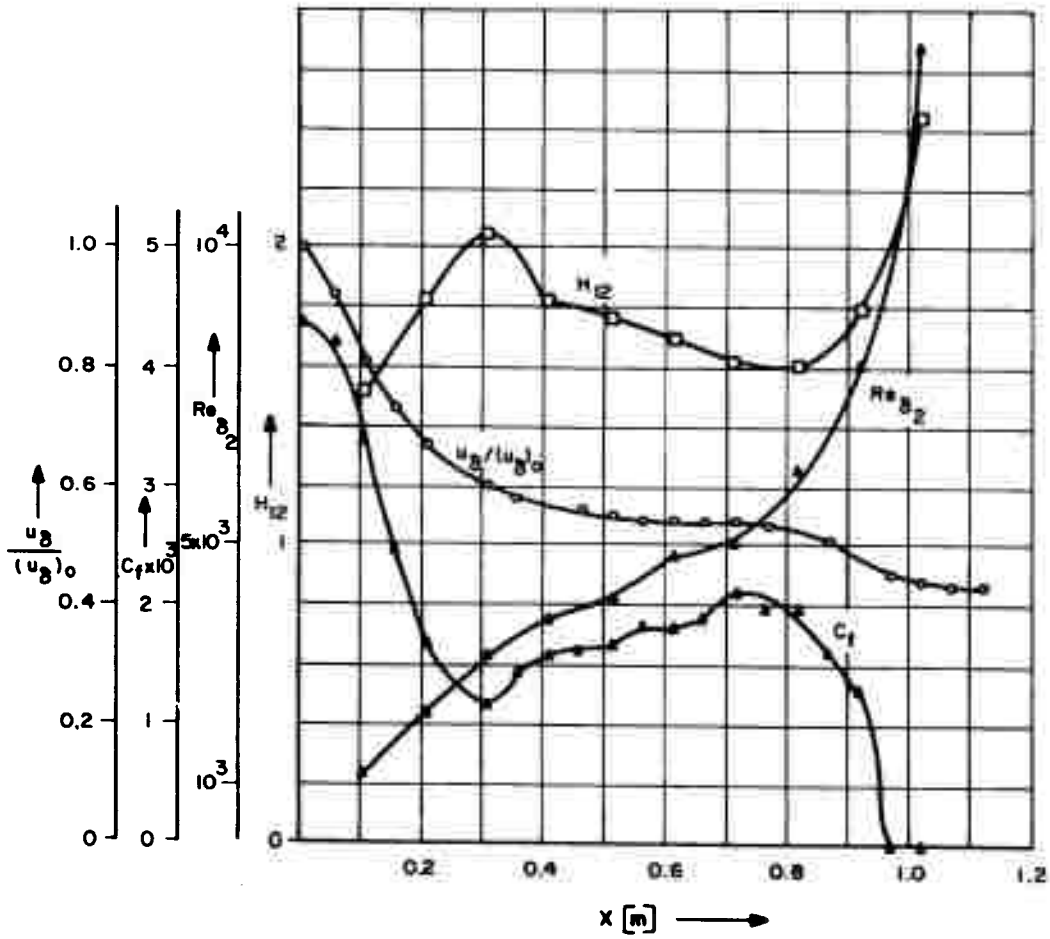

FIG. 14 REYNOLDS NUMBER, VELOCITY, SKIN FRICTION, AND H_{12} DISTRIBUTIONS (RUN III)

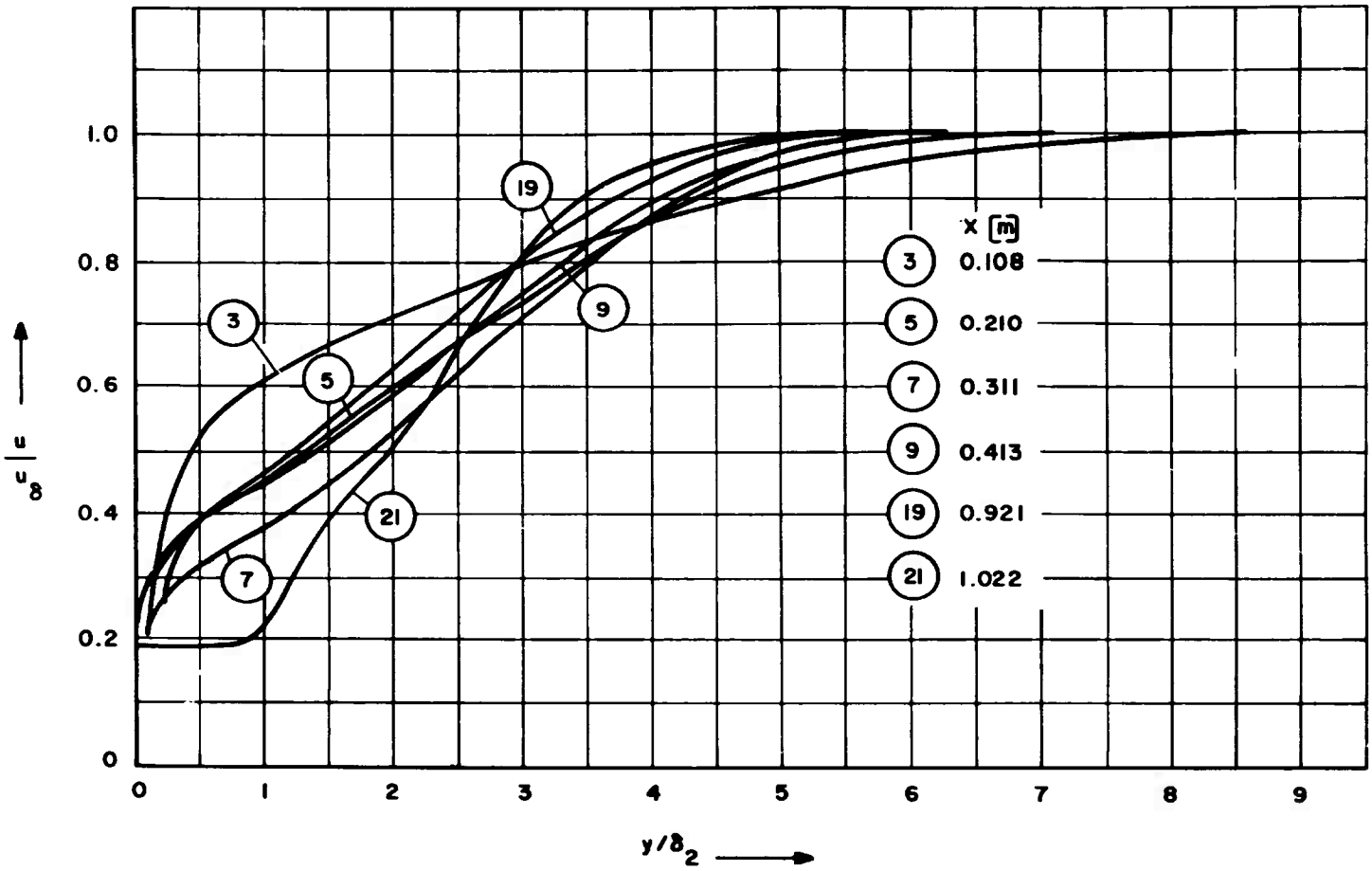

FIG.15 VELOCITY PROFILES IN A TURBULENT BOUNDARY LAYER (RUN III)

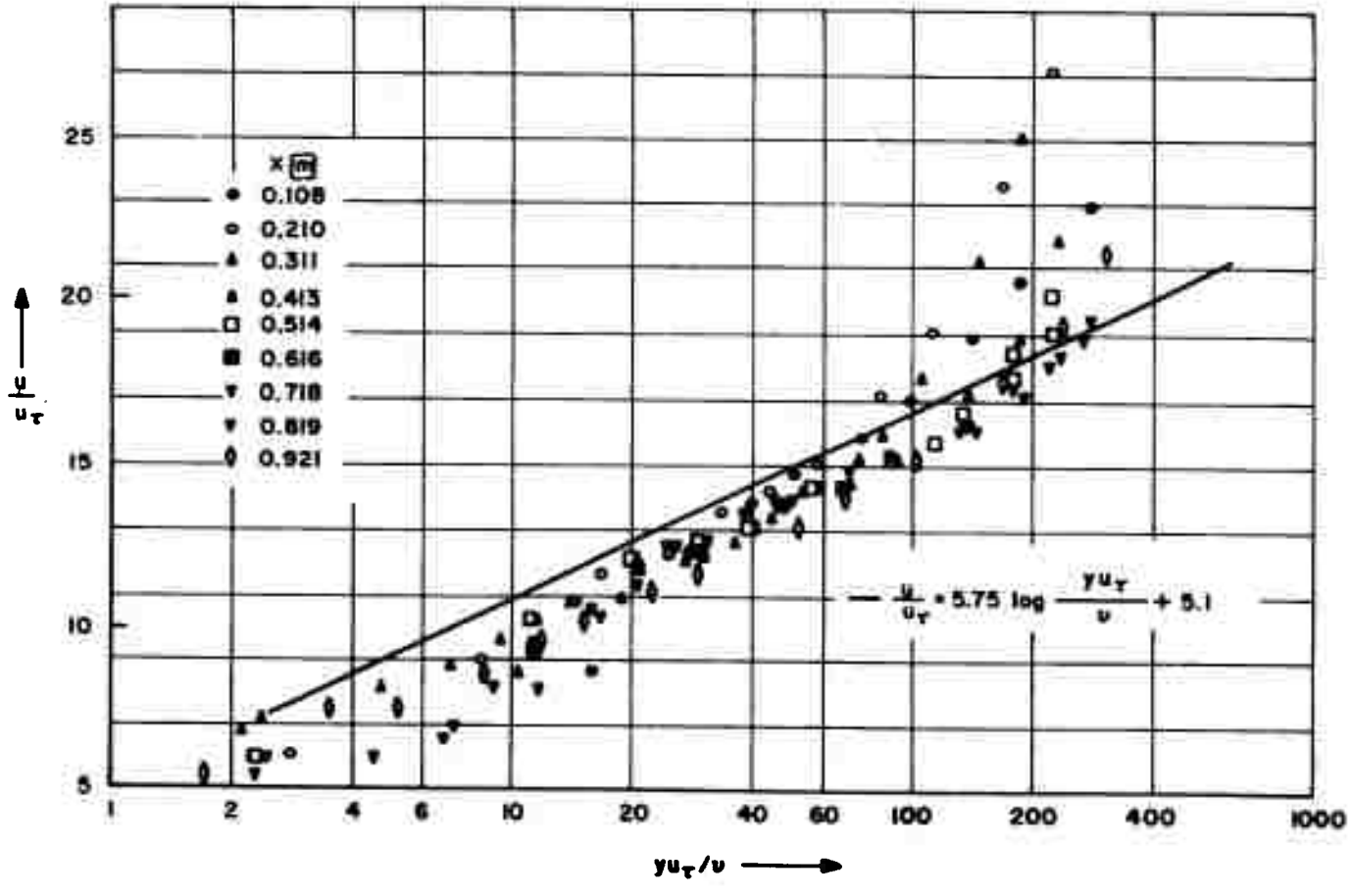

FIG.16 UNIVERSAL SEMILOGARITHMIC LAW OF VELOCITY PROFILES (RUN III)

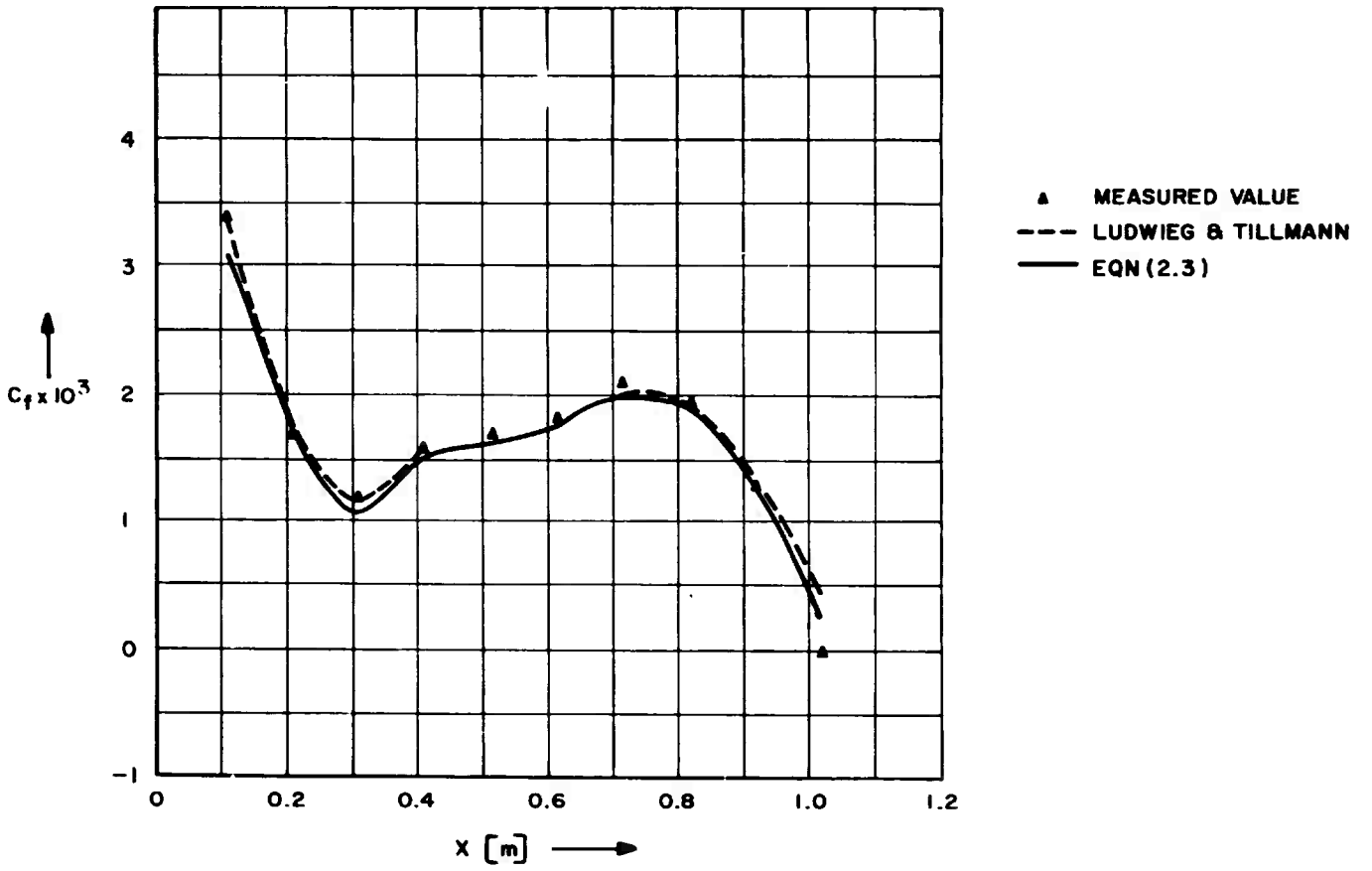

FIG.17 EXPERIMENTAL AND THEORETICAL WALL SHEAR STRESS (RUN III)

Unclassified

Security Classification

DOCUMENT CONTROL DATA - R&D

(Security classification of title, body of abstract and indexing annotation must be entered when the overall report is classified)

1. ORIGINATING ACTIVITY *(Corporate author)*
Massachusetts Institute of Technology
Gas Turbine Laboratory
Cambridge, Massachusetts 02139

2a. REPORT SECURITY CLASSIFICATION

2b. GROUP

3. REPORT TITLE

"Experiments on Turbulent Boundary Layers along a Circular Cylinder with and without Separation"

4. DESCRIPTIVE NOTES *(Type of report and inclusive dates)*
Final Report

5. AUTHOR(S) *(Last name, first name, initial)*
Fernholz, Hans, and Gibson, Paul

6. REPORT DATE	7a. TOTAL NO. OF PAGES	7b. NO. OF REFS
July 1967		23

8a. CONTRACT OR GRANT NO.
Nonr 1841(91)

b. PROJECT NO.
DTMB - Bureau of Ships General Hydromechanics Research Program S-R009-01 01

c.

d.

9a. ORIGINATOR'S REPORT NUMBER(S)
Gas Turbine Laboratory Report # 91

9b. OTHER REPORT NO(S) *(Any other numbers that may be assigned this report)*

10. AVAILABILITY/LIMITATION NOTICES
Copies of this report may be obtained from the Clearing House for Federal Scientific and Technical Information, Sills Building, Springfield, Virginia 22151

11. SUPPLEMENTARY NOTES
None

12. SPONSORING MILITARY ACTIVITY
Bureau of Ships - David Taylor Model Basin

13. ABSTRACT

Experiments were conducted in a turbulent boundary layer near separation along a circular cylinder with the flow in the axial direction. The pressure gradient along the axis of the cylinder could be varied such that it was possible to maintain three boundary-layer configurations close to separation or with regions of reversed flow:

1. A turbulent boundary layer with skin friction zero;

2. A turbulent boundary layer with a separated region and reattachment further downstream with skin friction zero;

3. A turbulent boundary layer with a region of small but constant skin friction and normal separation.

Pressure and skin friction along the cylinder wall, as well as mean velocity profiles in the boundary layer, were measured.

DD FORM 1 JAN 64 1473

Unclassified

Security Classification

14. KEY WORDS	LINK A		LINK B		LINK C	
	ROLE	WT	ROLE	WT	ROLE	WT
Turbulent Boundary Layers						
Separation						
Adverse Pressure Gradients						
Skin Friction Measurements						

INSTRUCTIONS

1. ORIGINATING ACTIVITY: Enter the name and address of the contractor, subcontractor, grantee, Department of Defense activity or other organization *(corporate author)* issuing the report.

2a. REPORT SECURITY CLASSIFICATION: Enter the overall security classification of the report. Indicate whether "Restricted Data" is included. Marking is to be in accordance with appropriate security regulations.

2b. GROUP: Automatic downgrading is specified in DoD Directive 5200.10 and Armed Forces Industrial Manual. Enter the group number. Also, when applicable, show that optional markings have been used for Group 3 and Group 4 as authorized.

3. REPORT TITLE: Enter the complete report title in all capital letters. Titles in all cases should be unclassified. If a meaningful title cannot be selected without classification, show title classification in all capitals in parenthesis immediately following the title.

4. DESCRIPTIVE NOTES: If appropriate, enter the type of report, e.g., interim, progress, summary, annual, or final. Give the inclusive dates when a specific reporting period is covered.

5. AUTHOR(S): Enter the name(s) of author(s) as shown on or in the report. Enter last name, first name, middle initial. If military, show rank and branch of service. The name of the principal author is an absolute minimum requirement.

6. REPORT DATE: Enter the date of the report as day, month, year; or month, year. If more than one date appears on the report, use date of publication.

7a. TOTAL NUMBER OF PAGES: The total page count should follow normal pagination procedures, i.e., enter the number of pages containing information.

7b. NUMBER OF REFERENCES: Enter the total number of references cited in the report.

8a. CONTRACT OR GRANT NUMBER: If appropriate, enter the applicable number of the contract or grant under which the report was written.

8b, 8c, & 8d. PROJECT NUMBER: Enter the appropriate military department identification, such as project number, subproject number, system numbers, task number, etc.

9a. ORIGINATOR'S REPORT NUMBER(S): Enter the official report number by which the document will be identified and controlled by the originating activity. This number must be unique to this report.

9b. OTHER REPORT NUMBER(S): If the report has been assigned any other report numbers *(either by the originator or by the sponsor)*, also enter this number(s).

10. AVAILABILITY/LIMITATION NOTICES: Enter any limitations on further dissemination of the report, other than those imposed by security classification, using standard statements such as:

(1) "Qualified requesters may obtain copies of this report from DDC."

(2) "Foreign announcement and dissemination of this report by DDC is not authorized."

(3) "U. S. Government agencies may obtain copies of this report directly from DDC. Other qualified DDC users shall request through _____."

(4) "U. S. military agencies may obtain copies of this report directly from DDC. Other qualified users shall request through _____."

(5) "All distribution of this report is controlled. Qualified DDC users shall request through _____."

If the report has been furnished to the Office of Technical Services, Department of Commerce, for sale to the public, indicate this fact and enter the price, if known.

11. SUPPLEMENTARY NOTES: Use for additional explanatory notes.

12. SPONSORING MILITARY ACTIVITY: Enter the name of the departmental project office or laboratory sponsoring *(paying for)* the research and development. Include address.

13. ABSTRACT: Enter an abstract giving a brief and factual summary of the document indicative of the report, even though it may also appear elsewhere in the body of the technical report. If additional space is required, a continuation sheet shall be attached.

It is highly desirable that the abstract of classified reports be unclassified. Each paragraph of the abstract shall end with an indication of the military security classification of the information in the paragraph, represented as *(TS)*, *(S)*, *(C)* or *(U)*

There is no limitation on the length of the abstract. However, the suggested length is from 150 to 225 words.

14. KEY WORDS: Key words are technically meaningful terms or short phrases that characterize a report and may be used as index entries for cataloging the report. Key words must be selected so that no security classification is required. Identifiers, such as equipment model designation, trade name, military project code name, geographic location, may be used as key words but will be followed by an indication of technical context. The assignment of links, roles, and weights is optional.